

1 **Identifying decadal trends in deweathered concentrations of criteria air pollutants**  
2 **in Canadian urban atmospheres with machine learning approaches**

3  
4 Xiaohong Yao<sup>1,\*</sup>, Leiming Zhang<sup>2,\*</sup>

5 <sup>1</sup> Key Laboratory of Marine Environment and Ecology (MoE), Frontiers Science Center  
6 for Deep Ocean Multispheres and Earth System, and Sanya Oceanographic Institution,  
7 Ocean University of China, Qingdao 266100, China

8 <sup>2</sup>Air Quality Research Division, Science and Technology Branch, Environment and  
9 Climate Change Canada, Toronto, M3H 5T4, Canada

10 \*Corresponds to: [xhyao@ouc.edu.cn](mailto:xhyao@ouc.edu.cn), [leiming.zhang@ec.gc.ca](mailto:leiming.zhang@ec.gc.ca)

11  
12 **Abstract.** This study investigates long-term trends of criteria air pollutants, including  
13 NO<sub>2</sub>, CO, SO<sub>2</sub>, O<sub>3</sub> and PM<sub>2.5</sub>, and O<sub>x</sub> (=NO<sub>2</sub>+O<sub>3</sub>) measured in ten Canadian cities  
14 during the last two to three decades and associated driving forces in terms of emission  
15 reductions, perturbations due to varying weather conditions and large-scale wildfires,  
16 and changes in O<sub>3</sub> sources and sinks. Two machine learning methods, the random forest  
17 algorithm and boosted regression trees, were used to extract deweathered mixing ratios  
18 (or mass concentrations) of the pollutants. The Mann-Kendall trend test of the  
19 deweathered and original annual average concentrations of the pollutants showed that,  
20 on the time scale of 20 years or longer, perturbation due to varying weather conditions  
21 on the decade trends of the pollutants are minimal (within  $\pm 2\%$ ) in about 70% of the  
22 studied cases, although it might be larger (but at most 16%) in the remaining cases.  
23 NO<sub>2</sub>, CO and SO<sub>2</sub> showed decreasing trends in the last two to three decades in all the  
24 cities except CO in Montreal. O<sub>3</sub> showed increasing trends in all the cities except  
25 Halifax, mainly due to weakened titration reaction between O<sub>3</sub> and NO. O<sub>x</sub>, however,  
26 showed decreasing trends in all the cities except Victoria because the increase in O<sub>3</sub> is  
27 much less than the decrease in NO<sub>2</sub>. In three of the five eastern Canadian cities,  
28 emission reductions dominated the decreasing trends in PM<sub>2.5</sub>, but no significant trends

29 in PM<sub>2.5</sub> were observed in the other two cities. In five western Canadian cities,  
30 increasing or no significant trends in PM<sub>2.5</sub> were observed, likely due to unpredictable  
31 large-scale wildfires overwhelming or balancing the impacts of emission reductions on  
32 PM<sub>2.5</sub>. In addition, despite improving air quality during the last two decades in most  
33 cities, air quality health index of above 10 (representing very high-risk condition) still  
34 occasionally occurred after 2010 in western Canadian cities because of the increased  
35 large-scale wildfires.

36

37 **Keywords:** Atmospheric pollutants, trend analysis, machine learning, emission  
38 reduction, wildfire emission

## 39 **1 Introduction**

40 Criteria air pollutants can harm human health and the natural environment. According  
41 to Health Impacts of Air pollution in Canada 2021 Report (Health Canada, 2021), it is  
42 estimated that air pollution of NO<sub>2</sub>, O<sub>3</sub> and PM<sub>2.5</sub> caused 15,300 deaths per year,  
43 corresponding to 42 deaths per 100,000 population in Canada in 2016. To protect  
44 human health and the environment, the Canadian Council of Ministers of the  
45 Environment (CCME) developed the Canadian Ambient Air Quality Standards  
46 (CAAQS) for PM<sub>2.5</sub>, O<sub>3</sub>, SO<sub>2</sub> and NO<sub>2</sub>. CAAQS are supported by four colour-coded  
47 management levels with each management level being determined by the amount of a  
48 pollutant within an air zone, from which recommendations on air quality management  
49 actions are provided. Following this standard, multiphase mitigation measures have  
50 been implemented to largely reduce anthropogenic air pollutant emissions in recent  
51 decades (ECCC, 2021). Air quality in Canadian urban atmospheres well meets CAAQS  
52 in recent years, as reported in Air Quality - Canadian Environmental Sustainability  
53 Indicators (ECCC, 2023).

54

55 Nevertheless, the World Health Organization (WHO, 2021) updated the global air  
56 quality guidelines (AQG) on NO<sub>2</sub>, SO<sub>2</sub>, CO, O<sub>3</sub> and PM<sub>2.5</sub> in 2021, based on

57 accumulated strong evidence that air pollution can affect public health even at very low  
58 concentrations. In the WHO 2021 AQG, NO<sub>2</sub> annual average concentration is set as 10  
59 µg m<sup>-3</sup>, equivalent to ~ 5 ppb at annual average temperatures of 6-10 °C across Canada,  
60 annual average and 24-hour average PM<sub>2.5</sub> concentrations are set as 5 µg m<sup>-3</sup> and 15 µg  
61 m<sup>-3</sup>, respectively, and peak season mean 8-hr O<sub>3</sub> concentration is set as 60 µg m<sup>-3</sup>. An  
62 urgent issue for all areas of the world is to overcome challenges to further lower ambient  
63 NO<sub>2</sub>, O<sub>3</sub> and PM<sub>2.5</sub> concentrations in order to meet the WHO 2021 AQG (Dabek-  
64 Zlotorzynska et al., 2019; Griffin et al., 2020; Xu et al., 2019; Jeong et al., 2020; Al-  
65 Abadleh et al., 2021; Wang et al., 2021; Zhang et al., 2022; Bowdalo et al., 2022).

66

67 In search of the most efficient mitigation measures for criteria pollutants, the  
68 effectiveness of existing measures on air pollution reduction needs to be first examined.  
69 For this purpose, long-term trends in concentrations of the criteria air pollutants need  
70 to be quantified and the driving forces of the trends, besides anthropogenic emission  
71 reductions, should be identified. Several studies have investigated the decadal trends of  
72 some criteria pollutants in Canada in the past decade. For example, Chan and Vet (2010)  
73 reported upward trends in O<sub>3</sub> mixing ratio from 1997-2006 at dozens of sites in Canada.  
74 Xu et al. (2019) and Zhang et al. (2022) also found increasing trends in O<sub>3</sub> mixing ratio  
75 from 1996-2016 at multiple sites in Windsor, Ontario, which was attributed to the  
76 reduced titration effect of NO with O<sub>3</sub>. They also reported that the 95<sup>th</sup> percentile O<sub>3</sub>  
77 mixing ratio exhibited a decreasing trend and attributed the decrease to anthropogenic  
78 emission reductions. Mitchell et al. (2021) reported that the 99<sup>th</sup> percentile O<sub>3</sub> mixing  
79 ratios exhibited a decreasing trend from 2000-2018 at urban and regional sites in Nova  
80 Scotia, but such a trend was not found for low-moderate percentile O<sub>3</sub> mixing ratios.  
81 Bari and Kindzierski (2016) found no significant trends in PM<sub>2.5</sub> mass concentration,  
82 although decreasing trends in organic carbon and elemental carbon from 2007-2014 in  
83 Edmonton. Jeong et al. (2020) reported 34% decrease in PM<sub>2.5</sub> mass concentration from  
84 2004-2017 in Toronto and attributed the decrease to the reduced coal-fired power plants  
85 emissions. Wang et al. (2022a) reported significant decreasing trends in organic and

86 elemental carbon in PM<sub>2.5</sub> from 2003-2019 at seven urban sites in Canada. Studies on  
87 other criteria pollutants are very limited (Feng et al., 2020; Jeong et al.; 2020).

88  
89 O<sub>3</sub> mixing ratios, especially at high levels, are strongly affected by meteorological  
90 conditions, and thus, trends on the decadal scale can be perturbed by varying weather  
91 conditions from year to year (Simon et al., 2015; Xing et al., 2015; Ma et al., 2021; Lin  
92 et al., 2022). Inter-annual variations of weather conditions also have strong impact on  
93 the decadal trends of other criteria pollutants (Lin et al., 2022). Air quality models are  
94 useful tools to analyze emission-driven air quality trends and meteorological impacts  
95 (Foley et al., 2015; Astitha et al., 2017; Vu et al., 2019), but most modeling results suffer  
96 from large uncertainties which could exceed changes in annual means of simulated  
97 pollutant concentrations. Machine learning techniques such as the random forest (RF)  
98 algorithm and boosted regression trees (BRTs) have been demonstrated to be a powerful  
99 tool to decouple impacts of emission changes and perturbations from varying weather  
100 and/or meteorological conditions, enabling the derivation of deweathered trends in air  
101 pollutants concentrations (Grange et al., 2018; Grange and Carslaw, 2019; Ma et al.,  
102 2021; Mallet, 2021; Shi and Brasseur, 2020; Wang et al., 2020; Munir et al., 2021;  
103 Lovric et al., 2021; Hou et al., 2022; Lin et al., 2022). The advantages and limitations  
104 of RF algorithm and BRTs have been described in detail in earlier studies (Grange et  
105 al., 2018; Grange and Carslaw, 2019). Briefly, BRTs method is fast to train and make  
106 prediction, but suffers heavily from overfitting, which may result in unreliable  
107 predictions. RF method can control the overfitting, but yields a poor prediction for  
108 outliers in large percentiles. Thus, using two methods with different strengths and  
109 weaknesses, although their predictions are similar in many ways, can constrain  
110 methodology uncertainties and better evaluate perturbations due to varying weather  
111 conditions than using only one method, as has been demonstrated in our earlier study  
112 (Lin et al., 2022).

113

114 This study attempts to deduct the perturbations due to varying weather conditions on

115 the observed mixing ratios (or mass concentrations) of some criteria air pollutants in  
116 Canada during the past two to three decades and thereby investigates their emission-  
117 driven trends. We used the RF algorithm and BRTs to generate the deweathered mixing  
118 ratios (or concentrations) of NO<sub>2</sub>, SO<sub>2</sub>, CO, O<sub>3</sub>, O<sub>x</sub> and PM<sub>2.5</sub> during the past decades  
119 in ten cities equally distributed in eastern and western Canada. Considering that the  
120 machine learning methods may suffer from the weakness in accurately predicting large  
121 percentile concentrations of the studied criteria air pollutants, we also applied our  
122 previously developed identical-percentile autocorrelation analysis method to better  
123 quantify the perturbations due to extreme events such as large-scale wildfires on large  
124 percentile PM<sub>2.5</sub> concentrations (Yao and Zhang, 2020; Lin et al., 2022). The Mann-  
125 Kendall (M-K) trend test was then employed to resolve the trends in the deweathered  
126 mixing ratios (or mass concentrations). Pearson correlation analysis was further  
127 conducted for the deweathered and original mixing ratios (or mass concentrations) of  
128 the air pollutants against the corresponding provincial-level emissions. City-level  
129 emissions were used in the analysis in cases with large differences between air pollutant  
130 concentrations and provincial-level emissions. In addition, the Air Quality Health Index  
131 (AQHI, [https://weather.gc.ca/airquality/pages/index\\_e.html](https://weather.gc.ca/airquality/pages/index_e.html)), a health protection tool  
132 designed in Canada to advise the public to adjust outdoor activities based on air  
133 pollution levels, was also analyzed with particular attention to the trends with AQHI  
134 being above 7 and 10, respectively. This study provides a thorough assessment of the  
135 emission-driven trends in the studied criteria pollutants on the time scale of two to three  
136 decades across Canadian urban atmospheres, knowledge from which is much needed  
137 in developing future emission control policies of the concerned pollutants.

## 138 **2 Methodology**

### 139 **2.1 Monitoring sites and data sources**

140 Ten major cities, including five in eastern Canada (Halifax, Quebec City, Montreal,  
141 Toronto and Hamilton) and five in western Canada (Winnipeg, Calgary, Edmonton,  
142 Vancouver and Victoria), from the National Air Pollution Surveillance (NAPS) program

143 are selected for investigating decadal trends of the monitored criteria pollutants (Table  
144 S1). The NAPS program has long-term air quality data of a uniform standard across  
145 Canada (Dabek-Zlotorzynska et al., 2011, 2019; Jeong et al., 2020; Yao and Zhang,  
146 2020; Wang et al., 2021, 2022a). The NAPS program includes both continuous and  
147 time-integrated measurements of gaseous and particulate air pollutants. Continuous  
148 data are available as hourly concentrations and are quality-assured as specified in the  
149 Ambient Air Monitoring and Quality Assurance/Quality Control Guidelines  
150 (<https://open.canada.ca/data/en/dataset/1b36a356-defd-4813-acea-47bc3abd859b>).

151  
152 Multiple monitoring sites exist in most cities, but only one urban background site was  
153 selected in each city mentioned above based on the following criteria: with the most  
154 complete dataset of the five selected criteria pollutants (NO<sub>2</sub>, CO, SO<sub>2</sub>, O<sub>3</sub> and PM<sub>2.5</sub>),  
155 with the longest data record, and with valid data in each year (Table S1). In cases with  
156 a data gap longer than a year, e.g., in Quebec City, Halifax and Calgary, data at a nearby  
157 urban background site (within 1 km) were then used to fill the gap. If no site within 1  
158 km is available, then the data gap is left unfilled. SO<sub>2</sub>, CO, NO<sub>x</sub> and PM<sub>2.5</sub> emission  
159 data at the provincial level in Canada are obtained from  
160 [https://www.canada.ca/en/environment-climate-change/services/environmental-](https://www.canada.ca/en/environment-climate-change/services/environmental-indicators/air-pollutant-emissions.html)  
161 [indicators/air-pollutant-emissions.html](https://www.canada.ca/en/environment-climate-change/services/environmental-indicators/air-pollutant-emissions.html). City-level air pollutant emissions from various  
162 [registered facilities since 2002 were obtained from](https://www.canada.ca/en/services/environment/pollution-waste-management/national-pollutant-release-inventory.html)  
163 [https://www.canada.ca/en/services/environment/pollution-waste-](https://www.canada.ca/en/services/environment/pollution-waste-management/national-pollutant-release-inventory.html)  
164 [management/national-pollutant-release-inventory.html](https://www.canada.ca/en/services/environment/pollution-waste-management/national-pollutant-release-inventory.html).

165  
166 Besides the monitored criteria pollutants described above, AQHI is also calculated in  
167 this study at three-hour resolution using the following formula (Stieb et al., 2008; To et  
168 al., 2013):

169  $AQHI = (100/10.4) \times [(e^{0.000537 \times O_3} - 1) + (e^{0.000871 \times NO_2} - 1) + (e^{0.000537 \times PM_{2.5}} - 1)]$ , in which  
170 O<sub>3</sub> and NO<sub>2</sub> represent their respective three-hour average original mixing ratios (in ppb)  
171 and PM<sub>2.5</sub> represents its three-hour average original concentration (in µg m<sup>-3</sup>). The

172 calculated AQHI is rounded to the nearest positive integer. AQHI between 1-3  
173 represents excellent air quality that is safe for outdoor activities. Outdoor activities may  
174 be reduced at AQHI between 4-6 for certain population with some health issues. AQHI  
175 between 7-10 and >10 correspond to high and very high health risk conditions,  
176 respectively. Note that four alternative AQHI-Plus amendments have been proposed for  
177 wildfire seasons and the AQHI-Plus values are always larger than the corresponding  
178 AQHI values (Yao et al., 2020). One of AQHI-Plus amendments has been implemented  
179 in late 2016 in British Columbia. The AQHI-Plus amendments are not used in this study  
180 since it is not implemented across the whole Canada.

181

## 182 **2.2 Statistical analysis**

183 In this study, two popular machine learning packages, including the “rmweather” R  
184 package (Grange et al., 2018) and the “deweather” R package ( Carslaw and Ropkins,  
185 2012; Carslaw and Taylor, 2009), were used to perform the RF algorithm and the BRTs,  
186 respectively. Besides the monitored hourly average mixing ratio (or mass concentration)  
187 of a pollutant, temporal variables (hour, day, weekday, week and month) and  
188 meteorological parameters (wind speed, wind direction, ambient temperature, relative  
189 humidity and dew point) are also needed as additional independent inputs to the  
190 machining learning process. The hourly meteorological data were obtained from the  
191 meteorological observational station at a nearby airport in each city, which are  
192 accessible from the NOAA Integrated Surface Database (ISD) by using the “worldmet”  
193 R package (Carslaw, 2021). The meteorological data from the nearest airport in every  
194 city should reflect synoptic weather conditions, which have been used in existing  
195 machine learning studies (Vu et al., 2019; Mallet, 2020; Wang et al., 2020; Dai et al.,  
196 2021; Ma et al., 2021). Additional meteorological parameters such as boundary layer  
197 height, total cloud cover, surface net solar radiation, surface pressure, total precipitation  
198 and air mass clusters have also been used in some studies to improve the performance  
199 of the machine learning methods (Hou et al., 2022; Shi et al., 2021; Lin et al., 2022).  
200 These additional meteorological parameters were not included in the present study, but

201 could be included in future analyses. Nevertheless, good performance can still be  
202 achieved in the present study mainly because of multi-decade length of the datasets, as  
203 demonstrated by an example shown in Fig. 1. Note that the inputs for the two packages  
204 were randomly divided into two groups and the user cannot control the division, i.e.,  
205 the training dataset that used 80% of the data and a testing dataset that used the  
206 remaining 20%. Thus, the testing datasets were different between the RF algorithm and  
207 the BRTs. Note that all input parameters and output variables, i.e., the predicted hourly  
208 average mixing ratio (or mass concentration) of a pollutant, for testing were the same  
209 as those used for learning. Moreover, the training and testing were conducted for every  
210 pollutant at every site.

211

212 Five statistical metrics, including coefficient of determination ( $R^2$ ), root mean square  
213 error (RMSE), mean bias (MB), mean fractional bias (MFB) and mean fractional error  
214 (MFE), were calculated to evaluate the performance of the two machine learning  
215 methods. In the literature, criteria and goal values have not been set for the statistical  
216 metrics for the purpose of evaluating machine learning prediction performance.  
217 Alternatively, the criteria and goal values for MFE and MFB proposed by USEPA are  
218 adopted here, which are  $MFE \leq 75\%$  and  $MFB \leq \pm 60\%$  for the criteria value and  $MFE \leq 50\%$   
219 and  $MFB \leq \pm 30\%$  for the goal value (USEPA, 2007).

220

221 Fig. 1 shows predictions against observations of  $\text{NO}_2$  mixing ratio in Halifax using the  
222 testing datasets during 1996-2017, as an example for evaluating the performance of the  
223 two machine learning methods (P value  $< 0.01$  for all the correlation). MFB and MFE  
224 values were far below their respective goal values for both RF algorithm and BRTs set  
225 by USEPA.  $R^2$  and RMSE were 0.86 and 5.1, respectively, for both methods. MB is -  
226 0.04 for RF algorithm and 0.1 for BRTs. The values of these metrics indicated that the  
227 predictions well reproduced the observations. However, the two machine learning  
228 methods overall underpredicted  $\text{NO}_2$  mixing ratios to a small extent based on the  
229 regression lines slightly below the 1:1 line. The underestimation was mainly due to

230 sporadic large values in the measurement of NO<sub>2</sub> mixing ratio, which did not provide  
231 sufficient samples for the machine learning methods to learn and yield good predictions.  
232 For all the pollutants in all the cities investigated in this study, the machine learning  
233 predictions generally met the goal values set by USEPA, except for PM<sub>2.5</sub> in some  
234 western Canadian cities such as Calgary and Edmonton with the predictions only  
235 meeting criteria values because of the perturbation from large-scale wildfires.

236

237 Following the approach described in earlier studies (Hou et al., 2022; Lin et al., 2022),  
238 the two machine learning methods were run for 1000 times with meteorological  
239 variables randomly resampled from the entire datasets during the study period. The  
240 average model prediction from the 1000 model runs represents the meteorologically  
241 normalized pollutant concentration at a particular time. We also tested averaging 2000  
242 and 3000 model predictions, which produced consistent results with those of using 1000  
243 model predictions. Thus, averaging 1000 model predictions was used for  
244 meteorological normalization in this study.

245

246 As mentioned above, the machine learning methods suffer from the weakness in  
247 accurately predicting high concentration values in large percentiles. We thus applied  
248 the identical-percentile autocorrelation analysis method developed in our previous  
249 study to quantify the perturbations due to extreme events such as large-scale wildfires  
250 on the large percentile concentration values (Yao and Zhang, 2020; Lin et al., 2022).  
251 This method has five steps for data processing and analysis. The first step is to construct  
252 a long-term average data series at hourly resolution covering 365 days by averaging the  
253 corresponding hourly data from all the years of the study period. The second step is to  
254 pair a data series at any given year to the long-term average data series, and if there  
255 were any data gaps (missing hours) in the former data series, data for these hours in the  
256 latter series were also removed so that the two data series have exactly the same size.  
257 The third step is to rearrange all the hourly data from the smallest to the largest value  
258 in each of the data series generated in step 2, and then conduct correlation analysis

259 between the pair of data series. Inflection points in the large and small percentile zone  
260 were first visibly identified/guessed, and referenced as upper and lower inflection  
261 points, respectively. The pair of data between the lower and upper inflection points were  
262 correlated repeatedly by varying values of the two inflection points in search for highest  
263  $R^2$  values. The fourth step is to predict the large percentile values exceeding the upper  
264 inflection point using the regression equation with the highest  $R^2$  generated in step 3.  
265 The final step is to obtain the perturbations due to extreme events on the large percentile  
266 concentrations by subtracting the observed values from the predicted values.

267

268 Fig. 2 shows three examples calculating the perturbations due to varying weather  
269 conditions and large-scale wildfires on the large percentile concentrations of  $PM_{2.5}$  in  
270 1998, 1999 and 2019 in Edmonton. Large-scale wildfires occurred in 1998 and 2019  
271 (Fig. S1), but no record in 1999. In 1998, data points outside the 4.5<sup>th</sup>-94<sup>th</sup> percentile  
272 range were screened out through steps 1-3, and the remaining data points were used to  
273 obtain a regression equation, which shows  $[PM_{2.5}]_{data\ in\ 1998} = [PM_{2.5}]_{long-term\ average} \times 3.9-$   
274  $18$  ( $R^2=0.96$ ,  $P<0.01$ ) (Fig. 2a).  $[PM_{2.5}]_{data\ in\ 1998}$  and  $[PM_{2.5}]_{long-term\ average}$  represent the  
275 same identical percentile values of  $PM_{2.5}$  in re-organized data series of 1998 and the  
276 long-term average through steps 1-3, respectively. The similar definition is applicable  
277 for  $[PM_{2.5}]_{data\ in\ 1999}$  and  $[PM_{2.5}]_{data\ in\ 2019}$  presented below. In 1999, data points within  
278 the 4.5<sup>th</sup>-99.7<sup>th</sup> percentile range resulted in a regression equation of  $[PM_{2.5}]_{data\ in\ 1999} =$   
279  $[PM_{2.5}]_{long-term\ average} \times 3.1-15$  ( $R^2=0.97$ ,  $P<0.01$ ) (Fig. 2c). In 2019, data points within  
280 the 5.4<sup>th</sup>-96<sup>th</sup> percentile range resulted in  $[PM_{2.5}]_{data\ in\ 2019} = [PM_{2.5}]_{long-term\ average} \times 2.2-$   
281  $12$  ( $R^2=0.94$ ,  $P<0.01$ ) (Fig. 2e). Note that step 3 is critical to obtain these excellent  
282 correlations (Fig. 2a, 2c and 2e) as compared with those absent of step 3 (Fig. 2b, 2d  
283 and 2f).

284

285 The perturbation due to the extreme weather conditions or the extreme events on the  
286 100<sup>th</sup> percentile  $PM_{2.5}$  value, i.e., the maximum value in this study, at a particular year  
287 (y) can be calculated as:

288  $[PM_{2.5}]_{\text{perturbation at } 100^{\text{th}}, y} = [PM_{2.5}]_{\text{predicted at } 100^{\text{th}}, y} - [PM_{2.5}]_{\text{observed at } 100^{\text{th}}, y}$

289  $[PM_{2.5}]_{\text{predicted at } 100^{\text{th}}, y} = [PM_{2.5}]_{\text{long-term average at } 100^{\text{th}}} \times k_y + b_y$

290 where  $[PM_{2.5}]_{\text{observed at } 100^{\text{th}}, y}$  represents the 100<sup>th</sup> percentile  $PM_{2.5}$  value observed in y  
291 year, and  $k_y$  and  $b_y$  represent the slope and intercept, respectively, of the regression  
292 equation with the highest  $R^2$  in the y year generated through steps 1-3. Similarly, the  
293 perturbation inherent from the large percentile values from the final upper inflection  
294 point ( $m^{\text{th}}$ ) to 100<sup>th</sup> percentile in a particular year can be calculated as:

295  $[PM_{2.5}]_{\text{perturbation at } \geq m^{\text{th}}, y} = [PM_{2.5}]_{\text{predicted at } \geq m^{\text{th}}, y} - [PM_{2.5}]_{\text{observed at } \geq m^{\text{th}}, y}$

296  $[PM_{2.5}]_{\text{predicted at } m^{\text{th}}, y} = [PM_{2.5}]_{\text{long-term average at } m^{\text{th}}} \times k_y + b_y$

297 The calculated values from  $[PM_{2.5}]_{\text{perturbation at } \geq m^{\text{th}}, y}$  to  $[PM_{2.5}]_{\text{perturbation at } 100^{\text{th}}, y}$  in the y  
298 year were averaged as  $[PM_{2.5}]_{\text{perturbation average}, y}$ . The perturbation contribution to the  
299 corresponding original annual average equals to  $[PM_{2.5}]_{\text{perturbation average}, y} \times (1-m\%)$  in y  
300 year, and the values were  $3.0 \mu\text{g m}^{-3}$  in 1998,  $0.2 \mu\text{g m}^{-3}$  in 1999 and  $1.7 \mu\text{g m}^{-3}$  in 2019  
301 in Edmonton, corresponding to strong, minimal and moderate perturbations,  
302 respectively, from large wildfires.

303

304 The M-K trend test is a non-parametric test applicable to any type of data distribution  
305 and is employed to resolve the trends in the time series of the deweathered and original  
306 annual average concentration of each pollutant. Qualitative trends revealed by the M-  
307 K trend test include 1) an increasing or decreasing trend with a P value of  $<0.05$ , and 2)  
308 no significant trend including a probably increasing or decreasing trend, a stable trend,  
309 and a no-trend with all the other conditions (Aziz et al., 2003; Kampata et al., 2008;  
310 Yao and Zhang, 2020). The extracted trends and associated driving factors are discussed  
311 in detail below.

312

### 313 **3. Results**

#### 314 *3.1 Trends in deweathered and original $NO_2$ mixing ratios*

315 Fig. 3a and 3b show decadal variations in the original annual averages of  $NO_2$  mixing  
316 ratios in the ten Canadian cities. The BRTs-deweathered and RF-deweathered hourly

317 averages of NO<sub>2</sub> mixing ratios are shown in Fig S2, in which the deweathered results  
318 were also interpreted in terms of increased or reduced emissions of NO<sub>x</sub>. The decadal  
319 trends resulted from annual averages of BRTs-deweathered, RF-deweathered and  
320 original NO<sub>2</sub> mixing ratios are listed in Table 1.

321

322 The deweathered and original annual average NO<sub>2</sub> mixing ratios in any of the 10 cities  
323 both showed consistent decreasing trends in the last 2-3 decades ( $P < 0.05$  through M-K  
324 trend test). The BRTs-deweathered and RF-deweathered annual averages highly  
325 correlated with the original values with  $R^2 > 0.95$  and  $P < 0.01$  (Table 1). The slopes of  
326 zero-intercept regression equations between the deweathered and original annual  
327 average NO<sub>2</sub> mixing ratios were mostly within 0.98-1.04, indicating  $\leq 4\%$  differences  
328 between the deweathered and original annual values. These results indicated that the  
329 perturbation due to varying weather conditions only exerted minor influences on the  
330 original annual averages. The only exception is the RF-deweathered annual averages in  
331 Halifax (with a slope of 1.08); however, this may not suggest that the perturbation due  
332 to varying weather conditions was as high as 8% since the BRTs-deweathered annual  
333 averages in the same city showed a slope of only 1.03, indicating that the uncertainties  
334 in the slope associated with the RF-deweathered averages can be as large as 5% (8%  
335 minus 3%) because of its poor prediction for large outlier values.

336

337 The annual decreasing rates in the deweathered and original NO<sub>2</sub> mixing ratios in the  
338 studied cities varied from 0.31 to 0.74 ppb year<sup>-1</sup>, and the overall percentage decreases  
339 ranged from 37% to 62% during the last two to three decades (Table 1). Our results  
340 suggested that varying weather conditions likely played a negligible role in the annual  
341 decreasing rates of NO<sub>2</sub> mixing ratio in two eastern (Montreal and Hamilton) and four  
342 western (Winnipeg, Calgary, Vancouver and Victoria) Canadian cities, as can be seen  
343 from the very close annual decreasing rates between the deweathered and original  
344 annual average mixing ratios, despite methodology uncertainties in generating  
345 deweathered mixing ratios as mentioned above. In the remaining four cities, the annual

346 decreasing rates were always larger in the original than the deweathered annual average  
347 NO<sub>2</sub> mixing ratio, with the largest differences in Toronto (0.07-0.10 ppb year<sup>-1</sup>),  
348 followed by Halifax (0.06-0.10 ppb year<sup>-1</sup>), Edmonton (0.06-0.08 ppb year<sup>-1</sup>) and  
349 Quebec City (0.02-0.07 ppb year<sup>-1</sup>), suggesting that varying weather conditions  
350 contributed appreciably to the annual decreasing rate. The annual decreasing rates were  
351 highly city-dependent, but there were no significant differences between eastern and  
352 western cities (P>0.05). With continuously decreasing NO<sub>2</sub> mixing ratios in the last  
353 decades (Fig. 3), annual average NO<sub>2</sub> fell to below 10 ppb by 2019 in half of the studied  
354 cities (Halifax, Montreal, Quebec City, Winnipeg and Victoria), meeting the WHO 2021  
355 guideline. Additional efforts are still needed to lower the NO<sub>2</sub> level in the rest of the  
356 cities, especially in Toronto and Edmonton in which annual average NO<sub>2</sub> were still as  
357 high as 15 ppb in 2019.

358

359 NO<sub>2</sub> in urban atmospheres were mainly formed by the rapid titration reaction of NO  
360 with O<sub>3</sub>, with NO largely released from anthropogenic emissions, especially the  
361 transport sector (Pappin et al., 2016; Casquero-Vera et al., 2019; Dabek-Zlotorzynska  
362 et al., 2019; Feng et a., 2020; Griffin et al., 2020; Al-Abadleh et al., 2021). The  
363 correlations between the annual average NO<sub>2</sub> mixing ratios and corresponding  
364 provincial NO<sub>x</sub> emissions were thereby analyzed below (Table 1). Note that the on-line  
365 air pollutant emission inventory in Canada reports the emissions since 1990 (ECCC,  
366 2021) so the correlation analysis only covers the period of 1990-2019. Strong  
367 correlations (R<sup>2</sup>=0.82-0.98) were obtained in all of the five eastern Canadian cities. The  
368 overall decreasing percentages of the deweathered and original NO<sub>2</sub> mixing ratios in  
369 Halifax and Quebec City were roughly the same as that of the provincial grand total  
370 NO<sub>x</sub> emissions and transportation NO<sub>x</sub> emissions, but in Montreal, Toronto and  
371 Hamilton the former decreasing percentages were smaller than the latter ones. In  
372 contrast, the overall decreasing percentages in NO<sub>2</sub> mixing ratio in the five western  
373 Canadian cities were substantially larger than the corresponding decreasing percentages  
374 of the provincial grand total NO<sub>x</sub> emissions and transportation NO<sub>x</sub> emissions, and the

375 correlation ( $R^2=0.54-0.94$ ) between  $\text{NO}_2$  mixing ratio and provincial emission were not  
376 as good as those in eastern cities. The extreme case occurred in Calgary, where  $\text{NO}_2$   
377 mixing ratio decreased by 31-33% during 1990-2007 when the grand total  $\text{NO}_x$   
378 emissions and transportation  $\text{NO}_x$  emissions in Alberta increased by 11% and 5%,  
379 respectively, noting that a much short period of data were used in this than other cities.  
380 The city-level  $\text{NO}_x$  emissions recorded from various facilities in Calgary increased from  
381 68 tons in 2002 to 262 tons in 2007 (Table S2), which cannot explain the decrease in  
382  $\text{NO}_2$  mixing ratios.

383

### 384 *3.2 Trends in deweathered and original mixing ratios of CO and SO<sub>2</sub>*

385 As mentioned earlier, CO and  $\text{SO}_2$  in Canadian cities well meet the CAAQS in recent  
386 years. The original annual average mixing ratios of CO and  $\text{SO}_2$  in the ten cities  
387 generally met the WHO 2021 air quality guidelines in the last decade, except  $\text{SO}_2$  in  
388 Hamilton (Fig. S4). Thus, the analysis results on deweathered and original mixing ratios  
389 of  $\text{SO}_2$  and CO in the nine cities and CO in Hamilton were only briefly summarized  
390 below, leaving  $\text{SO}_2$  in Hamilton to be discussed separately.

391

392 The annual averages of the deweathered CO mixing ratios were reasonably consistent  
393 with the original annual averages in five cities, e.g., the slopes of the deweathered  
394 mixing ratios against the original ones varied from 0.97 to 1.03 in Montreal, Hamilton,  
395 Winnipeg, Edmonton, Vancouver and Victoria, although somewhat large differences  
396 between the deweathered and original mixing ratios were seen in Quebec City with a  
397 slope of 1.12 (RF vs. Origin) and Toronto with a slope of 0.92 (BRTs vs. Origin). The  
398 original and deweathered annual averages of CO decreased by  $\geq 82\%$  in the last 2-3  
399 decades in six cities, including Halifax (90-92%), Calgary (90-91%), Winnipeg (84-  
400 88%), Edmonton (86-86%), Toronto (83-86%) and Vancouver (82-83%) (Table S3),  
401 followed by 66-70% in Hamilton and less than 60% in Quebec City (56-58%) and  
402 Victoria (57-59%). Large percentage decreases in baseline CO mixing ratios across  
403 North America were reported before (Zhou et al., 2017). The deweathered and original

404 annual averages of CO mixing ratio significantly correlated with the corresponding  
405 provincial grand total emissions and transportation emissions of CO ( $R^2 = 0.68-0.96$ ,  
406  $P < 0.01$ ) in these nine cities. The overall percentage decreases in CO mixing ratio in  
407 Quebec City and Victoria were approximately the same as those in the corresponding  
408 provincial transportation emissions of CO; however, the former percentage decreases  
409 were evidently larger than the latter ones in the other seven cities mentioned above. In  
410 Montreal, no significant trends were obtained in the deweathered and original CO  
411 mixing ratios during 1995-2010 ( $P > 0.05$ ), despite that the provincial total CO emissions  
412 and transportation CO emissions decreased by 37% and 53%, respectively, during the  
413 same period.

414

415 The deweathered and original annual average mixing ratios of  $SO_2$  decreased by 89-97%  
416 in the last 2-3 decades in four cities, including Winnipeg (95-97%), Vancouver (90-  
417 95%), Toronto (89-95%) and Halifax (90-93%), followed by 79-86% in Montreal, 78-  
418 85% in Quebec City, 73-82% in Victoria, 62-64% in Calgary and 52-55% in Edmonton  
419 (Table S4). Large percentage decreases in  $SO_2$  mixing ratio have been reported in rural  
420 atmospheres across North America during the last 2-3 decades (Xing et al., 2015; Feng  
421 et al., 2020). Since 1990, the overall decreasing percentages in  $SO_2$  mixing ratio in  
422 Halifax, Toronto, Calgary and Vancouver were evidently larger than those of the  
423 corresponding provincial grand total  $SO_2$  emissions. In Montreal, Quebec City,  
424 Winnipeg and Edmonton, the percentage decreases in  $SO_2$  mixing ratio were close to  
425 those in the corresponding provincial grand total  $SO_2$  emissions during the same periods.  
426 Although  $SO_2$  mixing ratio in Victoria decreased by 73-82% during 1999-2019, the  
427 corresponding provincial grand total  $SO_2$  emission did not decrease much during the  
428 same period. However, the city-level  $SO_2$  emissions from registered facilities in  
429 Victoria decreased from 217 tons in 2002 to near zero in 2019 (Table S2), supporting  
430 the decreases in  $SO_2$  mixing ratios. Note that the differences between the two  
431 deweathered mixing ratios of  $SO_2$  were enlarged to some extent in comparison with  
432 other pollutants, e.g., with the differences being 10-12% for  $SO_2$ , but only 2-5% for

433 NO<sub>2</sub> (as presented above), in Montreal, Toronto and Winnipeg. The increased  
434 uncertainties led to the difference between the RF-deweathered and original SO<sub>2</sub> mixing  
435 ratios being up to 16% in Winnipeg, based on the slope of 1.16 listed in Table S4. The  
436 difference between the BRTs-deweathered and original SO<sub>2</sub> mixing ratios was, however,  
437 only 4%, suggesting that the perturbation due to varying weather conditions might be  
438 within 4%-16%. Again, the RF algorithm suffers from the weakness in predicting large  
439 outlier values.

440

441 In Hamilton, the annual average of the deweathered SO<sub>2</sub> mixing ratios were highly  
442 consistent with those of the original data as indicated by the close to 1.0 slopes. The  
443 deweathered and original annual averages of SO<sub>2</sub> mixing ratios decreased by 23-28%  
444 during 1996-2019, which were substantially smaller than the 81% decrease of the  
445 corresponding provincial grand total SO<sub>2</sub> emissions during the same period. Such a  
446 large discrepancy indicates that the reduction in SO<sub>2</sub> emission in Hamilton likely  
447 substantially lagged behind the average provincial level. This is indeed the case since  
448 SO<sub>2</sub> emissions from registered facilities in Hamilton (Table S2) fluctuated around  
449  $8.67 \pm 1.75 \times 10^3$  tons year<sup>-1</sup> during 2002-2009 and then increased to  $1.14 \pm 0.13 \times 10^4$  tons  
450 year<sup>-1</sup> during 2010-2018. This also caused the weak correlations between annual  
451 average SO<sub>2</sub> mixing ratio in this city and provincial total SO<sub>2</sub> emission ( $R^2 = 0.42-0.57$ ,  
452  $P < 0.05$ ). In addition, the original annual average SO<sub>2</sub> mixing ratio increased from 3.2-  
453 3.5 ppb in 2016-2017 to 4.8-5.0 ppb in 2018-2019 when provincial total SO<sub>2</sub> emission  
454 changed little. Thus, reducing local SO<sub>2</sub> emissions in Hamilton is critical to further  
455 lower SO<sub>2</sub> mixing ratio in this city in order to meet the CAAQS and the WHO 2021  
456 guideline, despite the existence of other factors such as regional transport (Zhou et al.,  
457 2017; Ren et al., 2020).

458

### 459 *3.3 Trends in deweathered and original O<sub>3</sub> and O<sub>x</sub> mixing ratios*

460 The original annual averages of O<sub>3</sub> and O<sub>x</sub> are shown in Fig. S5 and the analysis results  
461 of deweathered and original annual averages are listed in Table S5. Increasing trends in

462 the deweathered and original annual average O<sub>3</sub> mixing ratio were obtained in nine  
463 cities during the last 2-3 decades, with Halifax as an only exception that showed no  
464 significant trend (P>0.05) during 2000-2017. Theoretically, the increasing trends in the  
465 O<sub>3</sub> mixing ratios could be caused by the enhanced tropospheric photochemical  
466 formation of O<sub>3</sub> and/or the weakened titration reaction between O<sub>3</sub> and NO due to the  
467 substantial reduction of NO emissions (Simon et al., 2015; Zhou et al., 2017; Sicard et  
468 al., 2020; Mitchell et al., 2021; Wang et al., 2022b) (more discussion in Section 4.2  
469 below). In contrast, the decreasing trends in the deweathered and original annual  
470 average O<sub>x</sub> mixing ratios were generally obtained, except in Victoria where there was  
471 no significant trend (P>0.05) during 2000-2017. The opposite long-term trends between  
472 O<sub>3</sub> and O<sub>x</sub> suggested that the increase in O<sub>3</sub> is much less than the decrease in NO<sub>2</sub>,  
473 which does not support the hypothesis of the enhanced tropospheric formation of O<sub>3</sub>.

474

475 The deweathered and original annual average O<sub>3</sub> mixing ratios increased by 10 ppb in  
476 Edmonton from 1981-2019, 8 ppb in Hamilton from 1996-2019 and Calgary from  
477 1986-2014, and <7 ppb in the other cities (Fig. S5, Table S5). The increased O<sub>3</sub> mixing  
478 ratio was likely caused by the reduced titration reaction between O<sub>3</sub> and NO,  
479 considering the reduced photochemical formation of O<sub>3</sub> in the troposphere (Simon et  
480 al., 2015; Xing et al., 2015). Varying weather conditions likely exerted a negligible  
481 influence on the decade increases in O<sub>3</sub> mixing ratio in Edmonton, Hamilton, Calgary  
482 and Vancouver on the basis of the almost identical increases in deweathered and original  
483 annual averages. However, the comparison between deweathered and original annual  
484 averages also showed that varying weather conditions did cause an increase of 2 ppb  
485 out of the total of 7 ppb increase in the original annual average O<sub>3</sub> in Winnipeg from  
486 1985-2018, and 1 ppb increase in Montreal from 1997-2010 and in Toronto from 2003-  
487 2019. In contrast, varying weather conditions likely caused 1 ppb decrease in Quebec  
488 City from 1995-2019 and in Victoria from 1999-2019.

489

490 The deweathered and original annual average O<sub>x</sub> mixing ratio decreased by 10-12 ppb

491 in Vancouver from 1986-2019, 10 ppb in Halifax from 2000-2019 and in Toronto from  
492 2003-2019, 8-10 ppb in Edmonton from 1981-2019 and <6 ppb in the other cities (Fig.  
493 S5 and Table S5). Based on the simultaneously monitored NO mixing ratios and the  
494 method reportedly used for estimating the primary NO<sub>2</sub> emission (Kurtenbach et al.,  
495 2012; Simon et al., 2015; Casquero-Vera et al., 2019; Xu et al., 2019), the reduced  
496 primary NO<sub>2</sub> emissions likely accounted for only 1-2 ppb decrease in O<sub>x</sub> in the ten cities  
497 and generally acted a minor contributor to the decrease in O<sub>x</sub>.

498

#### 499 *3.4 Trends in deweathered and original PM<sub>2.5</sub> mass concentrations*

500 Opposite decadal trends were observed between eastern and western Canadian cities in  
501 the deweathered and original PM<sub>2.5</sub> mass concentrations (Table 2, Fig. 3c, 3d and Fig  
502 S6). In eastern Canadian cities, either decreasing or no significant trends were obtained  
503 in the last two decades. The decreasing trends (P<0.05) were identified in the RF-  
504 deweathered, BRTs-deweathered and original annual average PM<sub>2.5</sub> in Montreal from  
505 2005-2019 and in Hamilton from 1998-2019. The overall decreases were only 2 µg m<sup>-3</sup>  
506 <sup>3</sup> with the decreasing rate of 0.22-0.25 µg m<sup>-3</sup> year<sup>-1</sup> in Montreal and 3-4 µg m<sup>-3</sup> and  
507 0.14-0.15 µg m<sup>-3</sup> year<sup>-1</sup> in Hamilton. The decreasing trends (P<0.05) were also  
508 identified in the RF-deweathered and BRTs-deweathered PM<sub>2.5</sub> in Toronto from 2000-  
509 2019 with an overall decrease of only 2 µg m<sup>-3</sup> and a decreasing rate of only 0.10-0.11  
510 µg m<sup>-3</sup> year<sup>-1</sup>. However, no significant trend (P>0.05) was identified in the original  
511 annual average PM<sub>2.5</sub> in Toronto, implying that the perturbation due to varying weather  
512 conditions likely cancelled out the mitigation effects of air pollutants. Note that there  
513 were no decreasing trends in the provincial total primary PM<sub>2.5</sub> emissions in Quebec  
514 and Ontario during the periods when PM<sub>2.5</sub> mass concentration decreased in the above-  
515 mentioned three cities. This was not surprising because the major chemical components  
516 in PM<sub>2.5</sub> were derived mainly from secondary sources (Dabek-Zlotorzynska et al., 2019;  
517 Jeong et al., 2020; Wang et al., 2021). The decreasing provincial emissions of SO<sub>2</sub>, NO<sub>x</sub>  
518 and volatile organic emissions in Quebec and Ontario likely have reduced the amounts  
519 of their oxidized products in PM<sub>2.5</sub> (Xing et al., 2015; Yao and Zhang, 2019, 2020; Feng

520 et al., 2020; Jeong et al., 2020; ECCC, 2021; Wang et al., 2021, 2022a). No significant  
521 trends ( $P > 0.05$ ) were identified in the deweathered and original  $PM_{2.5}$  concentrations  
522 in Halifax from 2008-2018 and in Quebec City from 1998-2019, which need further  
523 investigation.

524

525 In western Canadian cities, either increasing or no significant trends were extracted in  
526 the deweathered and original annual average  $PM_{2.5}$  mass concentrations. Increasing  
527 trends ( $P < 0.05$ ) were identified in the RF-deweathered, BRTs-deweathered and original  
528 annual average  $PM_{2.5}$  in Winnipeg from 2001-2018 with an overall increase of only 1-  
529  $2 \mu\text{g m}^{-3}$  and an increasing rate of  $0.09\text{-}0.10 \mu\text{g m}^{-3} \text{ year}^{-1}$ . Increasing trends ( $P < 0.05$ )  
530 were identified in the RF-deweathered and original annual average  $PM_{2.5}$  in Victoria  
531 from 1999-2019 with an overall increase of only  $1 \mu\text{g m}^{-3}$  and an increasing rate of  
532  $0.07\text{-}0.08 \mu\text{g m}^{-3} \text{ year}^{-1}$ , but no significant trend was identified in the BRTs-deweathered  
533 annual average  $PM_{2.5}$ . An increasing trend was obtained only in the RF-deweathered  
534 annual average  $PM_{2.5}$  in Vancouver from 2004-2019, and no significant trends were  
535 identified in the BRTs-deweathered and original annual average  $PM_{2.5}$ . The  
536 inconsistency between the trends extracted from the three different annual average  
537  $PM_{2.5}$  data series was mostly because of the small magnitudes of the actual interannual  
538 changes and thus the trends, which are on the same order of magnitude as the  
539 methodology uncertainties. Considering the decreasing trends in  $NO_2$ ,  $CO$  and  $SO_2$   
540 mixing ratios discussed above and the reported decreasing trends in secondary chemical  
541 components of  $PM_{2.5}$  in Western Canada (Wang et al., 2021, 2022a), the increasing  
542 trends in the deweathered and/or original annual average  $PM_{2.5}$  observed in some  
543 western Canadian cities were likely caused by increased natural emissions, such as from  
544 the increased large-scale wildfires in recent years.

545

546 It is noticed that a few spikes always appeared in the BRTs-deweathered  $PM_{2.5}$   
547 concentrations in the five western Canadian Cities since 2010 (Fig. S6). Most of these  
548 spikes were associated with large-scale wildfire emissions (Littell et al., 2009; Collier

549 et al., 2016; Landis et al., 2018; Matz et al., 2020). For example, wildfires caused large  
550 and rapid increases in PM<sub>2.5</sub> mass concentration from  $\leq 10 \mu\text{g m}^{-3}$  to  $>400 \mu\text{g m}^{-3}$  in  
551 Edmonton during 10-12 August 1998 and on 30 May 2019 (Fig. S1). During these  
552 periods, the BRTs method predicts the spikes of PM<sub>2.5</sub>. However, the RF method  
553 seemingly failed to learn the wildfire signals and missed predicting the spikes  
554 associated with largely increased natural emissions because of its inherent weakness.

555

556 To further explore the causes for the different trends in PM<sub>2.5</sub> between eastern and  
557 western Canadian cities, the 95<sup>th</sup>-100<sup>th</sup> percentile PM<sub>2.5</sub> mass concentration data in each  
558 year were averaged into annual value and were examined below. The top 5% PM<sub>2.5</sub>  
559 exhibited decreasing trends ( $P < 0.05$ ) in four eastern Canadian cities and no significant  
560 trend ( $P > 0.05$ ) in Halifax (Fig. S7). The decreasing trends further confirmed the  
561 mitigation effects of air pollutants on PM<sub>2.5</sub>. However, annual average PM<sub>2.5</sub> was still  
562 as high as  $8.8 \mu\text{g m}^{-3}$  in Hamilton in 2019,  $7.0\text{-}7.7 \mu\text{g m}^{-3}$  in Quebec City, Toronto and  
563 Montreal, and  $5.6 \mu\text{g m}^{-3}$  in Halifax. If keeping the same decreasing rates as mentioned  
564 above, it would take another 1-3 decades to lower annual average PM<sub>2.5</sub> by  $2\text{-}4 \mu\text{g m}^{-3}$   
565 in order to meet the WHO 2021 guideline.

566

567 No significant trends ( $P > 0.05$ ) were identified in the 95<sup>th</sup>-100<sup>th</sup> percentile PM<sub>2.5</sub> mass  
568 concentrations in the five western Canadian cities. Note that a large standard deviation  
569 of the 95<sup>th</sup>-100<sup>th</sup> percentile PM<sub>2.5</sub> mass concentration was found in some years in the  
570 five western cities, indicating a high variability. However, this is not the case in the  
571 eastern Canadian cities. The episodic PM<sub>2.5</sub> events likely canceled out the mitigation  
572 effects in the western Canadian cities. The annual average PM<sub>2.5</sub> were  $6.6\text{-}6.8 \mu\text{g m}^{-3}$  in  
573 2019 in Winnipeg, Edmonton and Victoria, which need great additional mitigation  
574 efforts in order to reduce to a level below  $5 \mu\text{g m}^{-3}$  in the presence of the episodes caused  
575 by natural emissions. Note that the annual average PM<sub>2.5</sub> was already lower than  $5 \mu\text{g m}^{-3}$   
576  $\text{m}^{-3}$  in Vancouver, and that the annual average was  $8.4 \mu\text{g m}^{-3}$  at the study site in Calgary  
577 in 2014. The value slightly decreased to  $7.6 \mu\text{g m}^{-3}$  in 2019 at another site  $\sim 5$  km from

578 the study site in Calgary.

579

### 580 *3.5 Trends in AQHI in the ten Canadian cities*

581 Decreasing trends in AQHI were obtained in nine cities ( $P < 0.05$ ), with Calgary as an  
582 only exception (Figs. S9 and S10). The annual average AQHI decreased by 8-29%  
583 during the last two decades to the levels of 1.8 to 3.0 during 2017-2019 in the nine cities.

584 In Calgary, the annual averages AQHI narrowed around  $3.4 \pm 0.2$  during 1998-2010. In  
585 the five eastern cities, AQHI above 10 occurred at  $< 0.3\%$  frequency before 2010, but  
586 none after 2010. AQHI between 7-10 occurred at  $< 4\%$  frequency before 2010, and  
587 below 0.5% after 2010. In the five western cities, AQHI above 10 occurred at  $< 0.3\%$   
588 frequency, and AQHI between 7-10 occurred at  $< 2\%$  frequency during the last two  
589 decades. Note that AQHI above 10 still occurred at  $< 0.3\%$  frequency even after 2010  
590 because of the large-scale wildfires. In fact, the occurrence frequencies of AQHI  
591 between 7-10 and above 10 were a bit higher after 2010 ( $< 0.3\%$ ) than before 2010 in  
592 Vancouver and Victoria due to the increased wildfire events in the most recent decade.

593

594 On seasonal average, AQHI above 10 occurred most in summer (from June to August)  
595 in most cities, e.g., Victoria (1.1%), Vancouver (0.8%), Edmonton (0.7%) and Winnipeg  
596 (0.1%) in 2018. AQHI above 10 also occurred in winter (from December to February  
597 next year) and spring (from March to May) in some cities, e.g., Edmonton (0.3% in the  
598 spring of 2019 and 0.1-0.3% in the winter of 2012-2013) and Winnipeg (0.1% in the  
599 spring of 2018).

600

## 601 **4. Discussion**

### 602 *4.1 Perturbations due to varying weather conditions on the decadal trends*

603 Perturbations due to varying weather conditions on the decadal trends of the studied  
604 pollutants are presented in detail in Section 3 above, and key findings are briefly  
605 summarized here. The perturbations are defined as the percentage differences between  
606 the trends of the original and deweathered annual average concentrations. In  $\sim 70\%$  of

607 the studies cases covering all the selected criteria pollutants in the ten cities, the  
608 perturbation due to varying weather conditions had an influence of within  $\pm 2\%$  on the  
609 decadal trends of the original annual averages over the 20-year period. In the remaining  
610 cases, relatively larger perturbations were identified, but at most 16%, keeping in mind  
611 that a portion of the percentage differences between the trends of the original and  
612 deweathered annual average concentrations was likely caused by errors inherent from  
613 BRTs and RF predictions.

614

615 Specifically, in all the cases except CO in Quebec City (for which the calculated  
616 perturbation is 7% from BRTs and 12% from RF), at least one of the two machining  
617 leaning methods generated a perturbation of smaller than 5%. For example, the top  
618 three largest perturbations obtained from using one of the two machining leaning  
619 methods were all for SO<sub>2</sub>, including 16% from RF in Winnipeg, 14% from BRTs in  
620 Montreal and 13% from RF from BRTs in Toronto; however, the corresponding  
621 perturbations from using another one of the two machining leaning methods were quite  
622 smaller (4%, 0.2% and 3%, respectively), indicating possible large methodology  
623 uncertainties. Thus, perturbations due to varying weather conditions should be  
624 generally small on the two-decade time scale in most cases.

625

#### 626 *4.2 Trend analysis of O<sub>3</sub> net sinks and sources*

627 As reported in literature, a large fraction of ground-level O<sub>3</sub> at middle-high latitude  
628 zones comes from secondary reactions associated with natural sources (Barrie et al.,  
629 1988; Van Dam et al., 2013; Cooper et al., 2005; Seinfeld and Pandis, 2006; Mitchell  
630 et al., 2021). The natural signal usually has a spring maximum related to stratosphere-  
631 troposphere exchange as well as increasing photochemistry, among other potential  
632 factors (Chan and Vet, 2010; Monks et al., 2015; Strode et al., 2018; Xu et al., 2019).  
633 The contributions from stratosphere-troposphere exchange are approximately 40 ppb,  
634 while the sinks associated with natural and anthropogenic factors in the atmospheric  
635 boundary layer may decrease the ground-level O<sub>3</sub> to levels lower than 40 ppb (Barrie

636 et al., 1988; Van Dam et al., 2013; Chan and Vet, 2010; Monks et al., 2015; Mitchell et  
637 al., 2021). On the other hand, enhanced tropospheric photochemical reactions under  
638 favorable meteorological conditions may increase the ground-level O<sub>3</sub> to levels higher  
639 than 40 ppb, causing severe O<sub>3</sub> pollution (Monks et al., 2015; Simon et al., 2015;  
640 Seinfeld and Pandis 2006; Xu et al., 2019). In fact, 40 ppb has been widely used as the  
641 threshold value for assessing O<sub>3</sub> impacts on ecosystem health (e.g., AOT40 index)  
642 (Avnery et al., 2011). Thus, O<sub>3</sub> data with mixing ratios lower and higher than 40 ppb  
643 were analyzed separately below, with the former case representing net O<sub>3</sub> sinks  
644 occurring in the atmospheric boundary layer and the latter one representing net O<sub>3</sub>  
645 sources occurring therein (Table 3).

646

647 In the cases with O<sub>3</sub> mixing ratios  $\geq$  40 ppb, the deweathered and original values,  
648 however, exhibited decreasing trends ( $P < 0.05$ ) in all of the five eastern cities and two  
649 western cities (Victoria and Vancouver) (Figs. 4 and S8 and Table 3). The overall  
650 decreases in O<sub>3</sub> with mixing ratios  $\geq$  40 ppb were 2 ppb in Halifax from 2000-2017, in  
651 Montreal and Quebec City from 1995-2019, and in Victoria from 1999-2019 (figure not  
652 provided), 4 ppb in Toronto from 2003-2019, 5-6 ppb in Hamilton from 1987-2019, and  
653 12 ppb in Vancouver from 1986-2019 (but only 2 ppb from 2000-2019). Again, a few  
654 spikes and troughs occurred in the BRTs-deweathered values possibly because of  
655 unpredictably increased and decreased emissions of O<sub>3</sub> precursors, respectively. In the  
656 cases with O<sub>x</sub> mixing ratios  $\geq$  40 ppb, the decreasing trends were obtained in all of the  
657 ten cities. These results further implied that the tropospheric photochemical formation  
658 of O<sub>3</sub> likely reduced in seven of the ten cities during the last two to three decades.

659

660 In the cases with O<sub>3</sub> mixing ratios  $\geq$  40 ppb in the remaining three western cities, the  
661 decreasing trends ( $P < 0.05$ ) were obtained in the BRTs-deweathered and original values  
662 and no significant trend ( $P > 0.05$ ) in the RF-deweathered values in Winnipeg; the  
663 decreasing trend was obtained only in the original values in Calgary; and no significant  
664 trends in the deweathered and original values in Edmonton. These trend results implied

665 that the responses of the fraction of O<sub>3</sub> to emission reductions of its precursors were too  
666 weak to be confirmed, especially in the presence of perturbation due to varying weather  
667 conditions.

668

669 In the cases with O<sub>3</sub> mixing ratios < 40 ppb, the trends were almost the same as those  
670 from using the full dataset of O<sub>3</sub> mixing ratios. This consistency suggested that the  
671 increasing trends in O<sub>3</sub> mixing ratio in the nine Canadian cities were mainly due to the  
672 reduced O<sub>3</sub> sinks.

673

#### 674 *4.3 The perturbation from large-scale wildfires on PM<sub>2.5</sub> trend in western Canadian* 675 *cities*

676 Wildfire emissions become important contributors to air pollution in North America  
677 with global warming and increased extreme weather conditions such as heatwaves and  
678 severe droughts (Andreae and Merlet, 2001; Littell et al., 2009; Marlon et al., 2013;  
679 Barbero et al., 2015; Abatzoglou and Williams, 2016; Randerson et al., 2017; Mardi et  
680 al., 2021). For example, Meng et al. (2019) estimated that wildfires accounted for 17.1%  
681 of the total population-weighted exposure to PM<sub>2.5</sub> for Canadians during 2013-2015  
682 and 2017-2018. The large contribution was not surprising because large wildfires can  
683 rapidly increase hourly PM<sub>2.5</sub> mass concentration from a few  $\mu\text{g m}^{-3}$  to  $>400 \mu\text{g m}^{-3}$   
684 (Landis et al., 2018 and Fig. S1). The estimated annual economic cost attributable to  
685 PM<sub>2.5</sub> pollution reached \$410M-\$1.8B for acute health impacts and \$4.3B-\$19B for  
686 chronic health impacts in western Canada (Landis et al., 2018; Matz et al., 2020). In the  
687 U.S., wildfire emissions were reported to account for up to 25% of annual primary  
688 PM<sub>2.5</sub> emissions (U.S. EPA, 2014).

689

690 Due to the wide occurrence of small-scale wildfires, most of the emitted air pollutants  
691 from these sources and subsequent long-range transport can be considered as natural  
692 background pollution. The key issue is to quantify the abnormally increased  
693 contributions from large-scale wildfires to annual average PM<sub>2.5</sub> in each year and their

694 perturbations on long-term trends in PM<sub>2.5</sub>. Using the method described in Section 2,  
695 the perturbation contributions in Winnipeg were estimated to be around  $0.5 \pm 0.4 \mu\text{g m}^{-3}$   
696 <sup>3</sup> in 2001-2018, with larger values of 1.1-1.3  $\mu\text{g m}^{-3}$  associated with large-scale wildfires  
697 in 2002, 2012 and 2018 (Fig. 5a). The larger perturbation contributions in 2012 and  
698 2018 indeed led to an increasing trend in PM<sub>2.5</sub> from 2001-2018 in this city (Table 2).  
699 The perturbation contributions were, however, smaller than  $0.2 \mu\text{g m}^{-3}$  in 2001, 2003,  
700 2005, 2006, 2008, 2009, 2014 and 2017, and such small values may be related to  
701 varying weather conditions rather than large-scale wildfires.

702

703 In Edmonton, the perturbation contributions were around  $1.0 \pm 0.9 \mu\text{g m}^{-3}$  in 1998-2019  
704 (Fig. 5b). However, the largest contribution was  $3.0 \mu\text{g m}^{-3}$  in 1998, followed by  $2.4 \mu\text{g m}^{-3}$   
705  $\text{m}^{-3}$  in 2018 and  $2.1 \mu\text{g m}^{-3}$  in 2004, respectively, because of large-scale wildfires. The  
706 perturbation contributions from large-scale wildfires were large enough to cancel out  
707 the mitigation effect of air pollutants on annual averages of PM<sub>2.5</sub> in Edmonton. In  
708 Calgary, the perturbation contributions were around  $1.2 \pm 0.7 \mu\text{g m}^{-3}$  in 1998-2013,  
709 depending on if large-scale wildfires occurred in any particular year. For example, the  
710 perturbation contributions were smaller than  $0.2 \mu\text{g m}^{-3}$  in 1999, 2007 and 2013, while  
711 the contributions reached 2.2-2.3  $\mu\text{g m}^{-3}$  in 1998 and 2010.

712

713 In Victoria, the perturbation contributions were around  $0.7 \pm 0.2 \mu\text{g m}^{-3}$  in 1998-2019.,  
714 The perturbation contribution in each year was, however, larger than  $0.4 \mu\text{g m}^{-3}$ ,  
715 suggesting that the wildfires were always important contributors. In Vancouver, the  
716 perturbation contributions largely decreased to  $0.3 \pm 0.5 \mu\text{g m}^{-3}$  in 2004-2019. However,  
717 the maximum value still reached  $1.7 \mu\text{g m}^{-3}$  in 2017, followed by  $1.4 \mu\text{g m}^{-3}$  in 2018  
718 and  $0.5 \mu\text{g m}^{-3}$  in 2015. The large perturbation likely overwhelmed or canceled out the  
719 effects of emission reductions on annual average PM<sub>2.5</sub>.

720

721 **5. Conclusions**

722 Through analysis of deweathered and original annual average concentrations of  
723 selected criteria air pollutants measured in ten major cities in Canada during the last 2-  
724 3 decades, we have generated the following decadal trends for these pollutants: 1)  
725 decreasing trends in NO<sub>2</sub>, CO and SO<sub>2</sub> mainly due to reduced primary emissions across  
726 Canada, except no significant trend in CO in Montreal; 2) increasing trends in O<sub>3</sub>  
727 mainly due to the reduced titration effect across Canada, except no significant trend in  
728 O<sub>3</sub> in Halifax; and 3) roughly opposite trends in PM<sub>2.5</sub> between eastern and western  
729 Canada, resulted from the combined effects of emission reductions and the occurrence  
730 of large-scale wildfires.

731

732 The overall percentage decrease in NO<sub>2</sub> during the last 2-3 decades among the 10 cities  
733 ranged from 37% to 62%, and the annual decreasing rates varied from 0.31 ppb year<sup>-1</sup>  
734 to 0.74 ppb year<sup>-1</sup>. The overall percentage decrease in CO varied from 57% to 92% and  
735 the annual decreasing rate ranged from 0.010 ppm year<sup>-1</sup> to 0.076 ppm year<sup>-1</sup> between  
736 nine cities. The corresponding numbers for SO<sub>2</sub> are from 23% to 93% and from 0.04  
737 ppb year<sup>-1</sup> to 0.63 ppb year<sup>-1</sup> among the 10 cities. By only considering O<sub>3</sub> mixing ratio  
738 ≥ 40 ppb, annual average O<sub>3</sub> decreased by 2-4 ppb in most cities during the past two-  
739 three decades, but not in Calgary and Edmonton, and no consistent decreasing trend  
740 was identified in Winnipeg, implying that the mitigation effects of air pollutants on O<sub>3</sub>  
741 were too weak to be confirmed.

742

743 The mitigation effects on PM<sub>2.5</sub> were detected on the basis of the identified decreasing  
744 trends in three of the five eastern cities regardless of using original or deweathered  
745 annual average data, but this is not the case in the other two eastern cities. In the five  
746 western cities, the perturbation due to large-scale wildfires greatly affected original  
747 annual average PM<sub>2.5</sub> and was large enough to cancel out the mitigation effects in some  
748 years, leading to no decreasing trends and in some cases even increasing trends.

749

750 Excluding Calgary, the annual average AQHI showed a significant decrease by 8-29%  
751 during the last two decades to levels between 1.8 and 3.0 in 2017-2019. However, large-  
752 scale wildfire events still occasionally elevated AQHI to a level of above 10 (very high  
753 risk) (<0.3% frequency) in western Canadian cities after 2010. Thus, large-scale  
754 wildfires have become a key factor in causing severe air pollution in Canadian cities,  
755 as was seen in the most recent very large-scale wildfires occurred in Canada from the  
756 later spring to the earlier summer in 2023 that resulted in severe air pollution across  
757 Canada and New York through long-range transport. Urgent work should be conducted  
758 for assessing the impacts of large-scale wildfires on human health and climate change,  
759 besides investigating their occurrence and control mechanisms and transport pathways.  
760 In-depth studies are also needed to explore the causes of the non-decreasing trends in  
761 O<sub>3</sub> with mixing ratios  $\geq 40$  ppb in some western Canadian cities, results from which are  
762 critical for making future control policies.

763

764 **Acknowledgement.** We greatly appreciate all the personnel of the NAPS Partners  
765 who operate the sites across Canada and collect the field samples, and the staff of the  
766 Analysis and Air Quality section in Ottawa for the laboratory chemical analyses and  
767 QA/QC of the data used in the present study. NPRI/APEI groups are also  
768 acknowledged for their efforts in generating emissions data across Canada.

769

770 *Data availability.* the data used in this paper are downloadable from  
771 <https://open.canada.ca/data/en/dataset/1b36a356-defd-4813-acea-47bc3abd859b>) and  
772 [https://www.canada.ca/en/environment-climate-change/services/environmental-](https://www.canada.ca/en/environment-climate-change/services/environmental-indicators/air-pollutant-emissions.html)  
773 [indicators/air-pollutant-emissions.html](https://www.canada.ca/en/environment-climate-change/services/environmental-indicators/air-pollutant-emissions.html).

774

775 *Author contributions.* XY and LZ designed the research, conducted analysis, and  
776 prepared the manuscript.

777

778 *Competing interests.* One of the coauthors is a member of the editorial board of ACP.

779

780

781 **References**

- 782 Abatzoglou, J. T. and Williams, A. P.: Impact of anthropogenic climate change on  
783 wildfire across western US forests, *Proc. Natl. Acad. Sci. USA.*, 113, 11770-11775,  
784 <https://doi.org/10.1073/pnas.1607171113>, 2016.
- 785 Al-Abadleh, H. A., Lysy, M., Neil, L., Patel, P., Mohammed, W., and Khalaf, Y.:  
786 Rigorous quantification of statistical significance of the COVID-19 lockdown effect  
787 on air quality: The case from ground-based measurements in Ontario, Canada, *J.*  
788 *Hazard. Mater.*, 413, 125445, <https://doi.org/10.1016/j.jhazmat.2021.125445>, 2021.
- 789 Andreae, M. O. and Merlet, P.: Emission of trace gases and aerosols from biomass  
790 burning, *Global. Biogeochem. Cy.*, 15, 955-966,  
791 <https://doi.org/10.1029/2000GB001382>, 2001.
- 792 Astitha, M., Luo, H., Rao, S. T., Hogrefe, C., Mathur, R., and Kumar, N.: Dynamic  
793 Evaluation of Two Decades of WRF-CMAQ Ozone Simulations over the  
794 Contiguous United States, *Atmos. Environ.*, 164, 102-116,  
795 <https://doi.org/10.1016/j.atmosenv.2017.05.020>, 2017.
- 796 Avnery, S., Mauzerall, D.L., Liu, J., Horowitz, L.W.: Global crop yield reductions due  
797 to surface ozone exposure: 2. Year 2030 potential crop production losses and  
798 economic damage under two scenarios of O<sub>3</sub> pollution. *Atmos. Environ.*, 45, 2297-  
799 2309, <https://doi.org/10.1016/j.atmosenv.2010.11.045>, 2011.
- 800 Aziz, J. J., Ling, M., Rifai, H. S., Newell, C. J., and Gonzales, J. R.: MAROS: a decision  
801 support system for optimizing monitoring plans, *Ground. Water.*, 41, 355-367,  
802 <https://doi.org/10.1111/j.1745-6584.2003.tb02605.x>, 2003.
- 803 Barbero, R., Abatzoglou, J. T., Larkin, N. K., Kolden, C. A., and Stocks, B.: Climate  
804 change presents increased potential for very large fires in the contiguous United  
805 States, *Int. J. Wildland. Fire.*, 24, <https://doi.org/10.1071/WF15083>, 2015.
- 806 Bari, M.A., Kindzierski, W.B. Eight-year (2007–2014) trends in ambient fine  
807 particulate matter (PM<sub>2.5</sub>) and its chemical components in the Capital Region of  
808 Alberta, Canada. *Environment Int.* 91, 122–132,  
809 <http://doi:10.1016/j.envint.2016.02.033>, 2016.
- 810 Barrie, L. A., Bottenheim, J. W., Schnell, R. C., Crutzen, P. J., and Rasmussen, R. A.:  
811 Ozone destruction and photochemical reactions at polar sunrise in the lower Arctic  
812 atmosphere, *Nature*, 334, 138-141, <https://doi.org/10.1038/334138A0>, 1988.
- 813 Bowdalo, D., Petetin, H., Jorba, O., Guevara, M., Soret, A., Bojovic, D., Terrado, M.,

814 Querol, X., and Pérez García-Pando, C.: Compliance with 2021 WHO air quality  
815 guidelines across Europe will require radical measures, *Environ. Res. Lett.*, 17,  
816 <https://doi.org/10.1088/1748-9326/ac44c7>, 2022.

817 Carslaw, D. C. and Taylor, P. J.: Analysis of air pollution data at a mixed source location  
818 using boosted regression trees, *Atmos. Environ.*, 43, 3563-3570,  
819 <https://doi.org/10.1016/j.atmosenv.2009.04.001>, 2009.

820 Carslaw, D. C. and Ropkins, K.: openair — An R package for air quality data analysis,  
821 *Environ. Modell. Softw.*, 27-28, 52-61,  
822 <https://doi.org/10.1016/j.envsoft.2011.09.008>, 2012.

823 Carslaw, D. C.: Worldmet: Import Surface Meteorological Data from NOAA Integrated  
824 Surface Database (ISD), R package version 0.9.5, [https://cran.r-](https://cran.r-project.org/package=worldmet)  
825 [project.org/package=worldmet](https://cran.r-project.org/package=worldmet). 2021.

826 Casquero-Vera, J. A., Lyamani, H., Titos, G., Borrás, E., Olmo, F. J., and Alados-  
827 Arboledas, L.: Impact of primary NO<sub>2</sub> emissions at different urban sites exceeding  
828 the European NO<sub>2</sub> standard limit, *Sci. Total. Environ.*, 646, 1117-1125,  
829 <https://doi.org/10.1016/j.scitotenv.2018.07.360>, 2019.

830 Chan, E. and Vet, R. J.: Baseline levels and trends of ground level ozone in Canada and  
831 the United States, *Atmos. Chem. Phys.*, 10, 8629-8647, [https://doi.org/10.5194/acp-](https://doi.org/10.5194/acp-10-8629-2010)  
832 [10-8629-2010](https://doi.org/10.5194/acp-10-8629-2010), 2010.

833 Collier, S., Zhou, S., Onasch, T. B., Jaffe, D. A., Kleinman, L., Sedlacek, A. J., 3rd,  
834 Briggs, N. L., Hee, J., Fortner, E., Shilling, J. E., Worsnop, D., Yokelson, R. J.,  
835 Parworth, C., Ge, X., Xu, J., Butterfield, Z., Chand, D., Dubey, M. K., Pekour, M.  
836 S., Springston, S., and Zhang, Q.: Regional Influence of Aerosol Emissions from  
837 Wildfires Driven by Combustion Efficiency: Insights from the BBOP Campaign,  
838 *Environ. Sci. Technol.*, 50, 8613-8622, <https://doi.org/10.1021/acs.est.6b01617>,  
839 2016.

840 Cooper, O. R.: A springtime comparison of tropospheric ozone and transport pathways  
841 on the east and west coasts of the United States, *J. Geophys. Res.*, 110,  
842 <https://doi.org/10.1029/2004JD005183>, 2005.

843 Dabek-Zlotorzynska, E., Celó, V., Ding, L., Herod, D., Jeong, C.-H., Evans, G., and  
844 Hilker, N.: Characteristics and sources of PM<sub>2.5</sub> and reactive gases near roadways  
845 in two metropolitan areas in Canada, *Atmos. Environ.*, 218,  
846 <https://doi.org/10.1016/j.atmosenv.2019.116980>, 2019.

847 Dabek-Zlotorzynska, E., Dann, T. F., Kalyani Martinelango, P., Celo, V., Brook, J. R.,  
848 Mathieu, D., Ding, L., and Austin, C. C.: Canadian National Air Pollution  
849 Surveillance (NAPS) PM<sub>2.5</sub> speciation program: Methodology and PM<sub>2.5</sub> chemical  
850 composition for the years 2003–2008, *Atmos. Environ.*, 45, 673–686,  
851 <https://doi.org/10.1016/j.atmosenv.2010.10.024>, 2011.

852 Dai, Q., Hou, L., Liu, B., Zhang, Y., Song, C., Shi, Z., Hopke, P. K., and Feng, Y.: Spring  
853 Festival and COVID-19 Lockdown: Disentangling PM Sources in Major Chinese  
854 Cities, *Geophys. Res. Lett.*, 48, e2021GL093403,  
855 <https://doi.org/10.1029/2021gl093403>, 2021.

856 ECCC, Environment and Climate Change Canada: Canadian Environmental  
857 Sustainability Indicators: Air pollutant emissions, available at:  
858 [https://www.canada.ca/en/environment-climate-change/services/environmental-](https://www.canada.ca/en/environment-climate-change/services/environmental-indicators/air-pollutant-emissions.html)  
859 [indicators/air-pollutant-emissions.html](https://www.canada.ca/en/environment-climate-change/services/environmental-indicators/air-pollutant-emissions.html), last access: 20 October 2023.

860 ECCC, Environment and Climate Change Canada: (2023) Canadian Environmental  
861 Sustainability Indicators: Air Quality. Available at:  
862 [www.canada.ca/en/environment-climate-change/services/environmental-](http://www.canada.ca/en/environment-climate-change/services/environmental-indicators/air-quality.html)  
863 [indicators/air-quality.html](http://www.canada.ca/en/environment-climate-change/services/environmental-indicators/air-quality.html)., last access 20 October 2023.

864 Feng, J., Chan, E., Vet, R. Air quality in the eastern United States and Eastern Canada  
865 for 1990–2015: 25 years of change in response to emission reductions of SO<sub>2</sub> and  
866 NO<sub>x</sub> in the region. *Atmos. Chem. Phys.*, 20, 3107–3134,  
867 <https://doi.org/10.5194/acp-20-3107-2020>

868 Foley, K. M., Hogrefe, C., Pouliot, G., Possiel, N., Roselle, S. J., Simon, H., and Timin,  
869 B.: Dynamic evaluation of CMAQ part I: Separating the effects of changing  
870 emissions and changing meteorology on ozone levels between 2002 and 2005 in the  
871 eastern US, *Atmos. Environ.*, 103, 247–255,  
872 <https://doi.org/10.1016/j.atmosenv.2014.12.038>, 2015.

873 Grange, S. K. and Carslaw, D. C.: Using meteorological normalisation to detect  
874 interventions in air quality time series, *Sci. Total. Environ.*, 653, 578–588,  
875 <https://doi.org/10.1016/j.scitotenv.2018.10.344>, 2019.

876 Grange, S. K., Carslaw, D. C., Lewis, A. C., Boleti, E., and Hueglin, C.: Random forest  
877 meteorological normalisation models for Swiss PM<sub>10</sub> trend analysis, *Atmos. Chem.*  
878 *Phys.*, 18, 6223–6239, <https://doi.org/10.5194/acp-18-6223-2018>, 2018.

879 Griffin, D., McLinden, C. A., Racine, J., Moran, M. D., Fioletov, V., Pavlovic, R.,

880 Mashayekhi, R., Zhao, X., and Eskes, H.: Assessing the Impact of Corona-Virus-19  
881 on Nitrogen Dioxide Levels over Southern Ontario, Canada, *Remote Sens-Basel*,  
882 12, <https://doi.org/10.3390/rs12244112>, 2020.

883 Health Canada. 2021. Health impacts of air pollution in Canada – Estimate of morbidity  
884 and premature mortality outcomes – 2021 report. Government of Canada. ISBN  
885 978-0-660-37331-7. 56 pp. [https://www.canada.ca/content/dam/hc-](https://www.canada.ca/content/dam/hc-sc/documents/services/publications/healthy-living/2021-health-effects-indoor-air-pollution/hia-report-eng.pdf)  
886 [sc/documents/services/publications/healthy-living/2021-health-effects-indoor-air-](https://www.canada.ca/content/dam/hc-sc/documents/services/publications/healthy-living/2021-health-effects-indoor-air-pollution/hia-report-eng.pdf)  
887 [pollution/hia-report-eng.pdf](https://www.canada.ca/content/dam/hc-sc/documents/services/publications/healthy-living/2021-health-effects-indoor-air-pollution/hia-report-eng.pdf)

888 Jeong, C.-H., Traub, A., Huang, A., Hilker, N., Wang, J. M., Herod, D., Dabek-  
889 Zlotorzynska, E., Celo, V., and Evans, G. J.: Long-term analysis of PM<sub>2.5</sub> from 2004  
890 to 2017 in Toronto: Composition, sources, and oxidative potential, *Environ. Pollut.*,  
891 263, <https://doi.org/10.1016/j.envpol.2020.114652>, 2020.

892 Kampata, J. M., Parida, B. P., and Moalafhi, D. B.: Trend analysis of rainfall in the  
893 headstreams of the Zambezi River Basin in Zambia, *Phys. Chem. Earth.*, 33, 621-  
894 625, <https://doi.org/10.1016/j.pce.2008.06.012>, 2008.

895 Kurtenbach, R., Kleffmann, J., Niedojadlo, A., and Wiesen, P.: Primary NO<sub>2</sub> emissions  
896 and their impact on air quality in traffic environments in Germany, *Environ. Sci.*  
897 *Eur.*, 24, <https://doi.org/10.1186/2190-4715-24-21>, 2012.  
898 <https://doi.org/10.1016/j.envpol.2020.115900>, 2021.

899 Landis, M. S., Edgerton, E. S., White, E. M., Wentworth, G. R., Sullivan, A. P., and  
900 Dillner, A. M.: The impact of the 2016 Fort McMurray Horse River Wildfire on  
901 ambient air pollution levels in the Athabasca Oil Sands Region, Alberta, Canada,  
902 *Sci. Total. Environ.*, 618, 1665-1676,  
903 <https://doi.org/10.1016/j.scitotenv.2017.10.008>, 2018.

904 Lin, Y., Zhang, L., Fan, Q., Meng, H., Gao, Y., Gao, H., and Yao, X.: Decoupling  
905 impacts of weather conditions on interannual variations in concentrations of criteria  
906 air pollutants in south China—constraining analysis uncertainties by using multiple  
907 analysis tools, *Atmos. Chem. Phys.*, 22, 16073–16090, [https://doi.org/10.5194/acp-](https://doi.org/10.5194/acp-22-16073-2022)  
908 [22-16073-2022](https://doi.org/10.5194/acp-22-16073-2022), 2022

909 Littell, J. S., McKenzie, D., Peterson, D. L., and Westerling, A. L.: Climate and wildfire  
910 area burned in western U.S. ecoprovinces, 1916-2003, *Ecol. Appl.*, 19, 1003-1021,  
911 <https://doi.org/10.1890/07-1183.1>, 2009.

912 Lovric, M., Pavlovic, K., Vukovic, M., Grange, S. K., Haberl, M., and Kern, R.:

913 Understanding the true effects of the COVID-19 lockdown on air pollution by  
914 means of machine learning, *Environ. Pollut.*, 274, 115900.

915 Ma, R., Ban, J., Wang, Q., Zhang, Y., Yang, Y., He, M. Z., Li, S., Shi, W., and Li, T.:  
916 Random forest model based fine scale spatiotemporal O<sub>3</sub> trends in the Beijing-  
917 Tianjin-Hebei region in China, 2010 to 2017, *Environ. Pollut.*, 276, 116635,  
918 <https://doi.org/10.1016/j.envpol.2021.116635>, 2021.

919 Mallet, M. D.: Meteorological normalisation of PM<sub>10</sub> using machine learning reveals  
920 distinct increases of nearby source emissions in the Australian mining town of  
921 Moranbah, *Atmos. Pollut. Res.*, 12, 23-35,  
922 <https://doi.org/10.1016/j.apr.2020.08.001>, 2021.

923 Mardi, A. H., Dadashazar, H., Painemal, D., Shingler, T., Seaman, S. T., Fenn, M. A.,  
924 Hostetler, C. A., and Sorooshian, A.: Biomass Burning Over the United States East  
925 Coast and Western North Atlantic Ocean: Implications for Clouds and Air Quality,  
926 *J. Geophys. Res.-Atmos.*, 126, <https://doi.org/doi:10.1029/2021JD034916>, 2021.

927 Marlon, J. R., Bartlein, P. J., Daniau, A.-L., Harrison, S. P., Maezumi, S. Y., Power, M.  
928 J., Tinner, W., and Vanni re, B.: Global biomass burning: a synthesis and review of  
929 Holocene paleofire records and their controls, *Quaternary. Sci. Rev.*, 65, 5-25,  
930 <https://doi.org/10.1016/j.quascirev.2012.11.029>, 2013.

931 Matz, C. J., Egyed, M., Xi, G., Racine, J., Pavlovic, R., Rittmaster, R., Henderson, S.  
932 B., and Stieb, D. M.: Health impact analysis of PM<sub>2.5</sub> from wildfire smoke in  
933 Canada (2013-2015, 2017-2018), *Sci. Total. Environ.*, 725, 138506,  
934 <https://doi.org/10.1016/j.scitotenv.2020.138506>, 2020.

935 Meng, J., Martin, R. V., Li, C., van Donkelaar, A., Tzompa-Sosa, Z. A., Yue, X., Xu, J.  
936 W., Weagle, C. L., and Burnett, R. T.: Source Contributions to Ambient Fine  
937 Particulate Matter for Canada, *Environ. Sci. Technol.*, 53, 10269-10278,  
938 <https://doi.org/10.1021/acs.est.9b02461>, 2019.

939 Mitchell, M., Wiacek, A., and Ashpole, I.: Surface ozone in the North American  
940 pollution outflow region of Nova Scotia: Long-term analysis of surface  
941 concentrations, precursor emissions and long-range transport influence, *Atmos.*  
942 *Environ.*, 261, <https://doi.org/10.1016/j.atmosenv.2021.118536>, 2021.

943 Monks, P. S., Archibald, A. T., Colette, A., Cooper, O., Coyle, M., Derwent, R., Fowler,  
944 D., Granier, C., Law, K. S., Mills, G. E., Stevenson, D. S., Tarasova, O., Thouret,  
945 V., von Schneidmesser, E., Sommariva, R., Wild, O., and Williams, M. L.:

946 Tropospheric ozone and its precursors from the urban to the global scale from air  
947 quality to short-lived climate forcer, *Atmos. Chem. Phys.*, 15, 8889-8973,  
948 <https://doi.org/10.5194/acp-15-8889-2015>, 2015.

949 Munir, S., Luo, Z., and Dixon, T.: Comparing different approaches for assessing the  
950 impact of COVID-19 lockdown on urban air quality in Reading, UK, *Atmos. Res.*,  
951 261, 105730, <https://doi.org/10.1016/j.atmosres.2021.105730>, 2021.

952 Pappin, A. J., Hakami, A., Blagden, P., Nasari, M., Szyszkowicz, M., and Burnett, R.  
953 T.: Health benefits of reducing NO<sub>x</sub> emissions in the presence of epidemiological  
954 and atmospheric nonlinearities, *Environ. Res. Lett.*, 11,  
955 <https://doi.org/10.1088/1748-9326/11/6/064015>, 2016.

956 Randerson, J.T., G.R. van der Werf, L. Giglio, G.J. Collatz, and P.S. Kasibhatla. 2017.  
957 Global Fire Emissions Database, Version 4.1 (GFEDv4). ORNL DAAC, Oak Ridge,  
958 Tennessee, USA. <https://doi.org/10.3334/ORNLDAAAC/1293>.

959 Ren, S., Stroud, C., Belair, S., Leroyer, S., Munoz-Alpizar, R., Moran, M., Zhang, J.,  
960 Akingunola, A., and Makar, P.: Impact of Urbanization on the Predictions of Urban  
961 Meteorology and Air Pollutants over Four Major North American Cities,  
962 *Atmosphere-Basel*, 11, <https://doi.org/10.3390/atmos11090969>, 2020.

963 Seinfeld, J.H. and Pandis, S.N. (2006) *Atmospheric Chemistry and Physics: From Air  
964 Pollution to Climate Change*. 2nd Edition, John Wiley & Sons, New York.

965 Shi, X. and Brasseur, G. P.: The Response in Air Quality to the Reduction of Chinese  
966 Economic Activities During the COVID-19 Outbreak, *Geophys. Res. Lett.*, 47,  
967 e2020GL088070, <https://doi.org/10.1029/2020GL088070>, 2020.

968 Shi, Z., Song, C., Liu, B., Lu, G., Xu, J., Van Vu, T., Elliott, R. J. R., Li, W., Bloss, W.  
969 J., and Harrison, R. M.: Abrupt but smaller than expected changes in surface air  
970 quality attributable to COVID-19 lockdowns, *Sci. Adv. Mater.*, 7,  
971 <https://doi.org/10.1126/sciadv.abd6696>, 2021.

972 Sicard, P., De Marco, A., Agathokleous, E., Feng, Z., Xu, X., Paoletti, E., Rodriguez, J.  
973 J. D., and Calatayud, V.: Amplified ozone pollution in cities during the COVID-19  
974 lockdown, *Sci. Total. Environ.*, 735, 139542,  
975 <https://doi.org/10.1016/j.scitotenv.2020.139542>, 2020.

976 Simon, H., Reff, A., Wells, B., Xing, J., and Frank, N.: Ozone trends across the United  
977 States over a period of decreasing NO<sub>x</sub> and VOC emissions, *Environ. Sci. Technol.*,  
978 49, 186-195, <https://doi.org/10.1021/es504514z>, 2015.

979 Stieb, D.M.; Burnett, R.T.; Smith-Doiron, M.; Brion, O.; Shin, H.H.; Economou, V.: A  
980 new multipollutant, no-threshold air quality health index based on short-term  
981 associations observed in daily time-series analyses, *J. Air Waste Manag. Assoc.* 58,  
982 435–450, <https://doi.org/10.3155/1047-3289.58.3.435>, 2008.

983 Strode, S. A., Ziemke, J. R., Oman, L. D., Lamsal, L. N., Olsen, M. A., and Liu, J.:  
984 Global changes in the diurnal cycle of surface ozone, *Atmos. Environ.*, 199, 323-  
985 333, <https://doi:10.1016/j.atmosenv.2018.11.028>, 2019.

986 To T., Shen S., Atenafu E.G., Guan J., McLimont S., Stocks B.: The Air Quality Health  
987 Index and asthma morbidity: A population-based study. *Environ Health Perspect.*  
988 121:46–52; <https://ehp.niehs.nih.gov/doi/10.1289/ehp.1104816>, 2013.

989 Van Dam, B., Helmig, D., Burkhardt, J. F., Obrist, D., and Oltmans, S. J.: Springtime  
990 boundary layer O<sub>3</sub> and GEM depletion at Toolik Lake, Alaska, *J. Geophys. Res.-*  
991 *Atmos.*, 118, 3382-3391, <https://doi.org/10.1002/jgrd.50213>, 2013.

992 Vu, T. V., Shi, Z., Cheng, J., Zhang, Q., He, K., Wang, S., and Harrison, R. M.:  
993 Assessing the impact of clean air action on air quality trends in Beijing using a  
994 machine learning technique, *Atmos. Chem. Phys.*, 19, 11303-11314,  
995 <https://doi.org/10.5194/acp-19-11303-2019>, 2019.

996 Wang, H., Zhang, L., Yao, X., Cheng, I., and Dabek-Zlotorzynska, E.: Identification of  
997 decadal trends and associated causes for organic and elemental carbon in PM<sub>2.5</sub> at  
998 Canadian urban sites, *Environ. Int.*, 159, 107031,  
999 <https://doi.org/10.1016/j.envint.2021.107031>, 2022a.

1000 Wang, H.; Lu, X.; Jacob, D.J.; Cooper, O.R.; Chang, K.L.; Li, K.; Gao, M.; Liu, Y.;  
1001 Sheng, B.; Wu, K.; Wu, T.; Zhang, J.; Sauvage, B.; Nédélec, P.; Blot, R.; Fan, S.  
1002 Global tropospheric ozone trends, attributions, and radiative impacts in 1995–2017:  
1003 an integrated analysis using aircraft (IAGOS) observations, ozonesonde, and multi-  
1004 decadal chemical model simulations. *Atmos. Chem. Phys.*, 22, 13753-13782,  
1005 <https://doi.org/10.5194/acp-22-13753-2022>, 2022b.

1006 Wang, H., Zhang, L., Cheng, I., Yao, X., and Dabek-Zlotorzynska, E.: Spatiotemporal  
1007 trends of PM<sub>2.5</sub> and its major chemical components at urban sites in Canada, *J.*  
1008 *Environ. Sci-China.*, 103, 1-11, <https://doi.org/10.1016/j.jes.2020.09.035>, 2021.

1009 Wang, Y., Wen, Y., Wang, Y., Zhang, S., Zhang, K. M., Zheng, H., Xing, J., Wu, Y., and  
1010 Hao, J.: Four-Month Changes in Air Quality during and after the COVID-19  
1011 Lockdown in Six Megacities in China, *Environ. Sci. Tech. Let.*, 7, 802-808,

1012 <https://doi.org/10.1021/acs.estlett.0c00605>, 2020.

1013 WHO, WHO global air quality guidelines: Particulate matter (PM<sub>2.5</sub> and PM<sub>10</sub>), ozone,  
1014 nitrogen dioxide, sulfur dioxide and carbon monoxide, ISBN-13: 978-92-4-003421-  
1015 1, <https://www.who.int/publications/i/item/9789240034228>, 2021.

1016 Xing, J., Mathur, R., Pleim, J., Hogrefe, C., Gan, C. M., Wong, D. C., Wei, C., Gilliam,  
1017 R., and Pouliot, G.: Observations and modeling of air quality trends over 1990–  
1018 2010 across the Northern Hemisphere: China, the United States and Europe, *Atmos.*  
1019 *Chem. Phys.*, 15, 2723-2747, <https://doi.org/10.5194/acp-15-2723-2015>, 2015.

1020 Xu, X., Zhang, T., and Su, Y.: Temporal variations and trend of ground-level ozone  
1021 based on long-term measurements in Windsor, Canada, *Atmos. Chem. Phys.*, 19,  
1022 7335-7345, <https://doi.org/10.5194/acp-19-7335-2019>, 2019.

1023 Yao, J., Stieb, D.M., Taylor, E., Henderson, S.: Assessment of the air quality health  
1024 index (AQHI) and four alternate AQHI-Plus amendments for wildfire seasons in  
1025 British Columbia. *Can J Public Health* 111, 96–106.  
1026 <https://doi.org/10.17269/s41997-019-00237-w>, 2020.

1027 Yao, X. and Zhang, L.: Causes of large increases in atmospheric ammonia in the last  
1028 decade across North America. *ACS Omega*, 11, 4(26), 22133-22142, <https://doi.org/10.1021/acsomega.9b03284>, 2019.

1030 Yao, X. and Zhang, L.: Decoding long-term trends in the wet deposition of sulfate,  
1031 nitrate, and ammonium after reducing the perturbation from climate anomalies,  
1032 *Atmos. Chem. Phys.*, 20, 721-733, <https://doi.org/10.5194/acp-20-721-2020>, 2020.

1033 Zhang, T., Xu, X., and Su, Y.: Long-term measurements of ground-level ozone in  
1034 Windsor, Canada and surrounding areas, *Chemosphere*, 294, 133636,  
1035 <https://doi.org/10.1016/j.chemosphere.2022.133636>, 2022.

1036 Zhou, Y., Mao, H., Demerjian, K., Hogrefe, C., and Liu, J.: Regional and Hemispheric  
1037 Influences on Temporal Variability in Baseline Carbon Monoxide and Ozone over  
1038 the Northeast US, *Atmos. Environ.* 164, 309-324,  
1039 <http://dx.doi.org/10.1016/j.atmosenv.2017.06.017>, 2017.

Table 1. Regression of (BRTs and RF) deweathered against original annual average NO<sub>2</sub> mixing ratios, annual decreasing rate (ppb year<sup>-1</sup>) and overall decreasing percentage (%) of deweathered and original NO<sub>2</sub> mixing ratios (P<0.05 for all the decreasing trends), correlation (R<sup>2</sup>) of deweathered and original NO<sub>2</sub> mixing ratios against provincial total NO<sub>x</sub> emissions and transportation NO<sub>x</sub> emissions (P<0.05 except those marked with “/” for which p>0.05), and percentage decreases (%) of the provincial total NO<sub>x</sub> emissions and transportation NO<sub>x</sub> emissions (P<0.05 for all the decreasing trends except increasing trends in NO<sub>x</sub> emission from 1990-2010 in Winnipeg and Calgary<sup>#</sup>) in ten Canadian cities during the last decades (<sup>##</sup>since 1990; bold font numbers represent cases with smaller decreasing percentages in NO<sub>2</sub> mixing ratios than in corresponding provincial emissions, italic numbers represent R<sup>2</sup>>0.8, and italic bold numbers represent an increasing trend).

| City                  | Regression of deweathered against original mixing ratio (P<0.01) |              | Annual decreasing rate (ppb year <sup>-1</sup> ) and overall decreasing percentage (%) (P<0.05) |                           |                           | Correlation (R <sup>2</sup> ) of mixing ratios against provincial total and transportation NO <sub>x</sub> emissions (P<0.05) |                             |                             | Percentage decreases (%) of provincial total and transportation emissions <sup>&amp;&amp;</sup> |
|-----------------------|--|--------------|---|---------------------------|---------------------------|---|-----------------------------|-----------------------------|---|
|                       | BRTs   | RF           | BRTs  | RF                        | original                  | BRTs  | RF                          | original                    |   |
| Halifax (1996-2017)   | y=1.03×<br>x   | y=1.08<br>×x | 0.49,<br>62   | 0.45,<br>58               | 0.55,<br>50               | <i>0.83,</i><br><i>0.84</i>   | <i>0.84,</i><br><i>0.85</i> | <i>0.86,</i><br><i>0.87</i> | 54, 56  |
| Montreal (1995-2019)  | y=0.99×<br>x   | y=1.04<br>×x | <i>0.34,</i><br><b>44</b>   | <i>0.32,</i><br><b>42</b> | <i>0.34,</i><br><b>39</b> | <i>0.90,</i><br><i>0.85</i>   | <i>0.91,</i><br><i>0.86</i> | <i>0.87,</i><br><i>0.82</i> | <b>47, 52</b>   |
| Quebec (1996-2019)    | y=0.98×<br>x   | y=1.02<br>×x | 0.44,<br>51   | 0.39,<br>45               | 0.46,<br>46               | <i>0.97,</i><br><i>0.97</i>   | <i>0.97,</i><br><i>0.98</i> | <i>0.95,</i><br><i>0.95</i> | 47, 52  |
| Toronto (2004-2019)   | y=1.02×<br>x   | y=1.04<br>×x | <i>0.67,</i><br><b>40</b>   | <i>0.64,</i><br><b>39</b> | <i>0.74,</i><br><b>37</b> | <i>0.96,</i><br><i>0.96</i>   | <i>0.97,</i><br><i>0.98</i> | <i>0.94,</i><br><i>0.94</i> | <b>52, 52</b>   |
| Hamilton (1996-2019)  | y=1.00×<br>x   | y=1.02<br>×x | <i>0.53,</i><br><b>42</b>   | <i>0.55,</i><br><b>44</b> | <i>0.54,</i><br><b>42</b> | <i>0.95,</i><br><i>0.97</i>   | <i>0.95,</i><br><i>0.96</i> | <i>0.92,</i><br><i>0.93</i> | <b>58, 57</b>   |
| Winnipeg (1984-2018)  | y=0.99×<br>x   | y=1.00<br>×x | 0.37,<br>57   | 0.34,<br>57               | 0.34,<br>50               | <i>0.90,</i><br><i>0.93</i>   | <i>0.91,</i><br><i>0.94</i> | <i>0.85,</i><br><i>0.89</i> | 43, 43 <sup>#</sup>   |
| Edmonton (1994-2019)  | y=1.02×<br>x   | y=1.00<br>×x | 0.45,<br>41   | 0.47,<br>40               | 0.53,<br>45               | <i>0.57,</i><br><i>0.73</i>   | <i>0.54,</i><br><i>0.73</i> | <i>0.63,</i><br><i>0.73</i> | 10, 29  |
| Calgary (1986-2007)   | y=1.00×<br>x   | y=1.01<br>×x | 0.60,<br>31   | 0.60,<br>32               | 0.61,<br>33               | /   | /                           | /                           | <b>-11, -5<sup>#</sup></b>  |
| Vancouver (1986-2019) | y=1.00×<br>x   | y=1.01<br>×x | 0.36,<br>49   | 0.36,<br>47               | 0.37,<br>49               | 0.63,<br>0.75   | 0.63,<br>0.74               | 0.54,<br>0.66               | 23, 27 <sup>##</sup>  |
| Victoria (1993-2019)  | y=1.01×<br>x   | y=1.02<br>×x | 0.31,<br>0.49   | 0.31,<br>0.45             | 0.31,<br>0.51             | 0.58,<br>0.69   | 0.58,<br>0.69               | 0.54,<br>0.65               | 23, 33 <sup>##</sup>  |

Table 2. Regression of (BRTs and RF) deweathered against original annual average PM<sub>2.5</sub> mass concentrations, annual decreasing rate ( $\mu\text{g m}^{-3} \text{ year}^{-1}$ ) and overall decrease ( $\mu\text{g m}^{-3}$ ) of deweathered and original PM<sub>2.5</sub> mass concentrations, and percentage decreases (%) of the provincial total PM<sub>2.5</sub> emissions in ten Canadian cities during the last decades (decreasing trends were obtained with  $P < 0.05$  except those marked with “/” for which  $P > 0.05$ ; and bold font numbers represent cases with increasing trends).

| City                  | Regression of deweathered against original mixing ratio ( $P < 0.01$ ) |                   | Annual decreasing rate ( $\mu\text{g m}^{-3} \text{ year}^{-1}$ ) and overall decrease ( $\mu\text{g m}^{-3}$ ) |                  |                  | Decreasing percentage (%) of provincial total PM <sub>2.5</sub> emissions |
|-----------------------|--|-------------------|---|------------------|------------------|---|
|                       | BRTs   | RF                | BRTs  | RF               | original         |   |
| Halifax (2008-2018)   | $y=1.00 \times x$  | $y=1.02 \times x$ | /   | /                | /                | 27  |
| Montreal (2005-2019)  | $y=1.00 \times x$  | $y=1.01 \times x$ | 0.24, 2   | 0.22, 2          | 0.25, 2          | /   |
| Quebec (1998-2019)    | $y=1.00 \times x$  | $y=1.01 \times x$ | /   | /                | /                | /   |
| Toronto (2000-2019)   | $y=1.00 \times x$  | $y=1.01 \times x$ | 0.11, 2   | 0.10, 2          | /                | /   |
| Hamilton (1998-2019)  | $y=1.00 \times x$  | $y=1.01 \times x$ | 0.15, 4   | 0.14, 3          | 0.15, 3          | /   |
| Winnipeg (2001-2018)  | $y=1.04 \times x$  | $y=1.04 \times x$ | <b>-0.10, -2</b>  | <b>-0.10, -2</b> | <b>-0.09, -1</b> | <b>-11</b>  |
| Edmonton (1998-2019)  | $y=1.01 \times x$  | $y=1.03 \times x$ | /   | /                | /                | <b>-40</b>  |
| Calgary (1998-2014)   | $y=1.00 \times x$  | $y=1.03 \times x$ | /   | /                | /                | <b>-38</b>  |
| Vancouver (2004-2019) | $y=0.99 \times x$  | $y=1.02 \times x$ | /   | <b>-0.08, -1</b> | /                | 28  |
| Victoria (1999-2019)  | $y=1.00 \times x$  | $y=1.03 \times x$ | /   | <b>-0.08, -1</b> | <b>-0.07, -1</b> | 42  |

Table 3. Trends in deweathered and original annual average O<sub>3</sub> and O<sub>x</sub> mixing ratios at levels below and above 40 ppb in ten Canadian cities during the last decades (#decreasing trends with P<0.05; ##no trend or stable trend with P>0.10; ###increasing trend with P<0.05).

|                       | O <sub>3</sub> |    |          |          |    |          | O <sub>x</sub> |    |          |          |    |          |
|-----------------------|----------------|----|----------|----------|----|----------|----------------|----|----------|----------|----|----------|
|                       | ≥ 40 ppb       |    |          | < 40 ppb |    |          | ≥ 40 ppb       |    |          | < 40 ppb |    |          |
|                       | BRTs           | RF | Original | BRTs     | RF | Original | BRTs           | RF | Original | BRTs     | RF | Original |
| Halifax (2000-2017)   | ↓#             | ↓  | ↓        | /##      | /  | /        | ↓              | ↓  | ↓        | ↓        | ↓  | ↓        |
| Montreal (1997-2010)  | ↓              | ↓  | ↓        | ↑###     | ↑  | ↑        | ↓              | ↓  | ↓        | /        | /  | /        |
| Quebec (1995-2019)    | ↓              | ↓  | ↓        | ↑        | ↑  | ↑        | ↓              | ↓  | ↓        | /        | ↓  | /        |
| Toronto (2003-2019)   | ↓              | ↓  | ↓        | ↑        | ↑  | ↑        | ↓              | ↓  | ↓        | ↓        | ↓  | ↓        |
| Hamilton (1996-2019)  | ↓              | ↓  | ↓        | ↑        | ↑  | ↑        | ↓              | ↓  | ↓        | /        | /  | /        |
| Winnipeg (1985-2018)  | ↓              | /  | ↓        | ↑        | ↑  | ↑        | ↓              | ↓  | ↓        | ↓        | ↓  | /        |
| Edmonton (1981-2019)  | /              | /  | /        | ↑        | ↑  | ↑        | ↓              | ↓  | ↓        | ↓        | ↓  | ↓        |
| Calgary (1986-2014)   | /              | /  | ↓        | ↑        | ↑  | ↑        | ↓              | ↓  | ↓        | ↓        | ↓  | ↓        |
| Vancouver (1986-2019) | ↓              | ↓  | ↓        | ↑        | ↑  | ↑        | ↓              | ↓  | ↓        | ↓        | ↓  | ↓        |
| Victoria (1999-2019)  | ↓              | ↓  | ↓        | ↑        | ↑  | ↑        | ↓              | ↓  | ↓        | /        | /  | /        |

## List of Figures

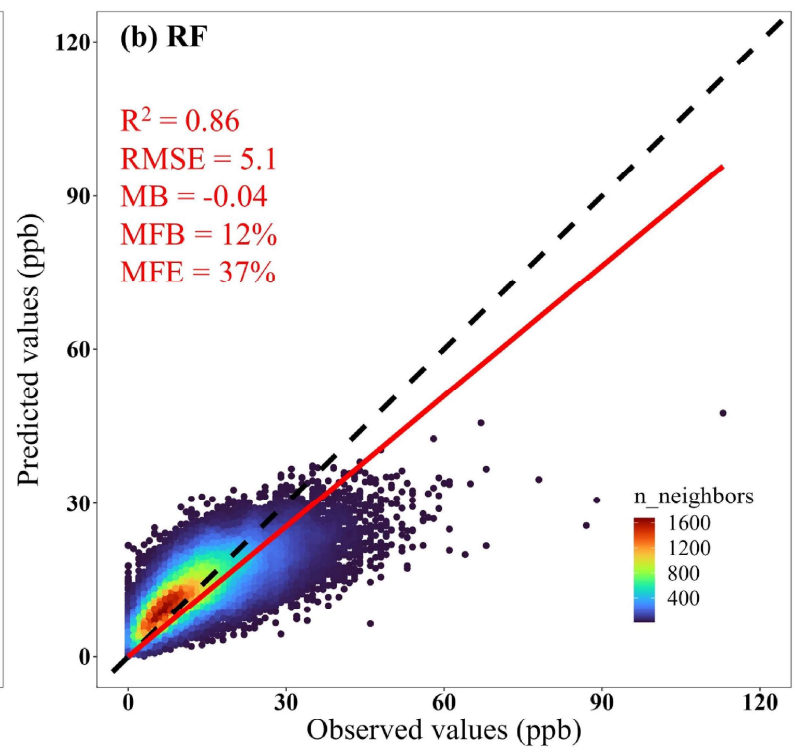
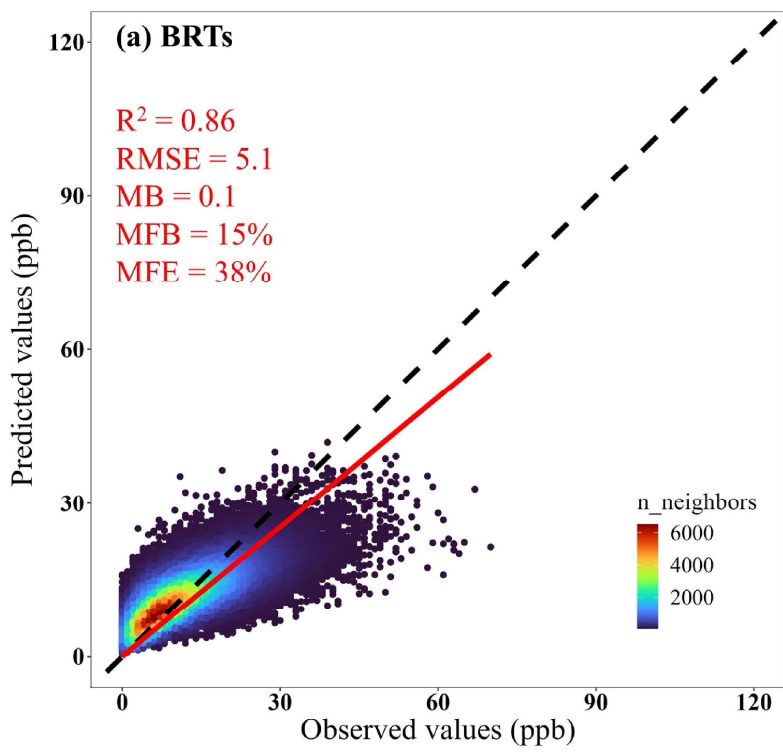
Fig. 1. Performance evaluation of the predicted NO<sub>2</sub> hourly mixing ratios by BRTs and RF algorithm against those observed in Halifax during 1996-2017. Red lines represent linear regression, and color bar reflects data number density. Note that different observational data sets are shown between (a) and (b) because the inputs for the two packages (BRTs and RF) are randomly divided into two groups for training and testing.

Fig. 2. Correlations between hourly PM<sub>2.5</sub> concentration in a single year and 22-year average PM<sub>2.5</sub> concentration in each hour of the year in Edmonton. Left columns show percentile series of PM<sub>2.5</sub> in 1998, 1999 and 2019, respectively, against the corresponding 22-year average series. Right column shows time series of PM<sub>2.5</sub> in 1998, 1999 and 2019, respectively, against the corresponding 22-year average series. Blue straight dashed lines in a, c and e represent the regression curves within linear ranges and their extensions out of the ranges; vertical arrows represent the distance of the predicted values from the regression curve. Blue straight lines and dark blue dashed lines in b, d and f represent the regression curves and 1:1 lines, respectively.

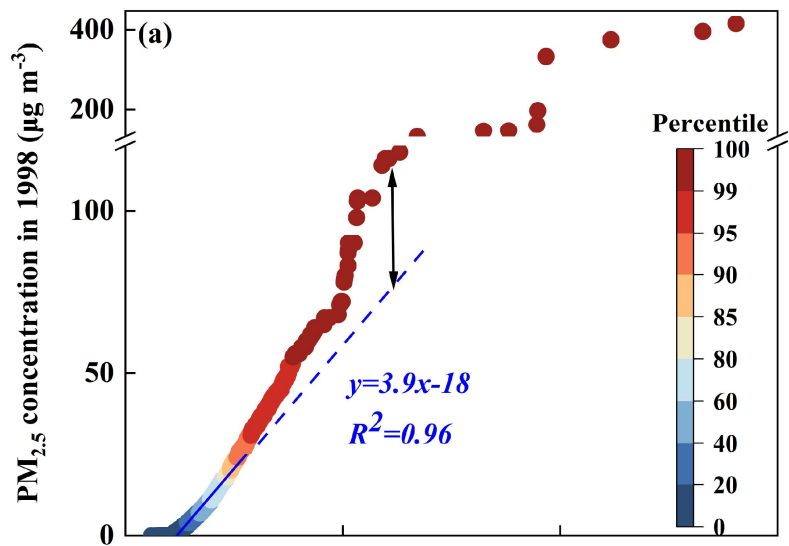
Fig. 3. Trends of original annual average NO<sub>2</sub> (upper row) and PM<sub>2.5</sub> (lower row) in five eastern (left column) and five western (right column) Canadian Cities.

Fig. 4 Deweathered hourly mixing ratios of O<sub>3</sub> (left column) and O<sub>x</sub> (right column) at levels  $\geq 40$  ppb in five eastern Canadian cities.

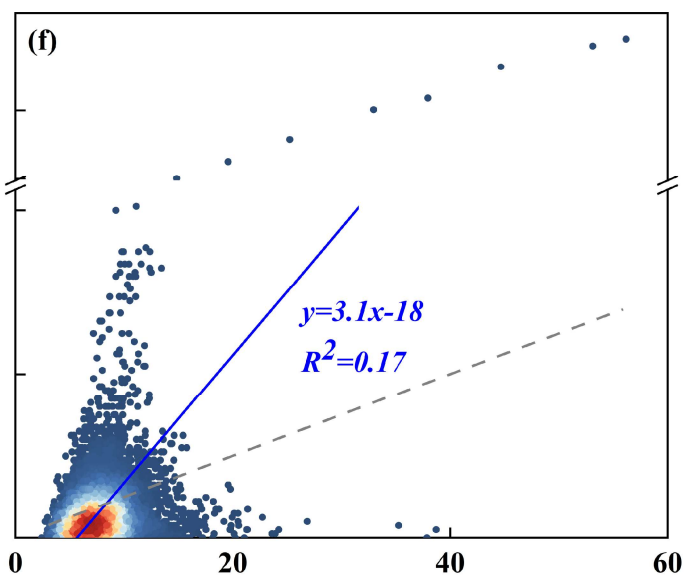
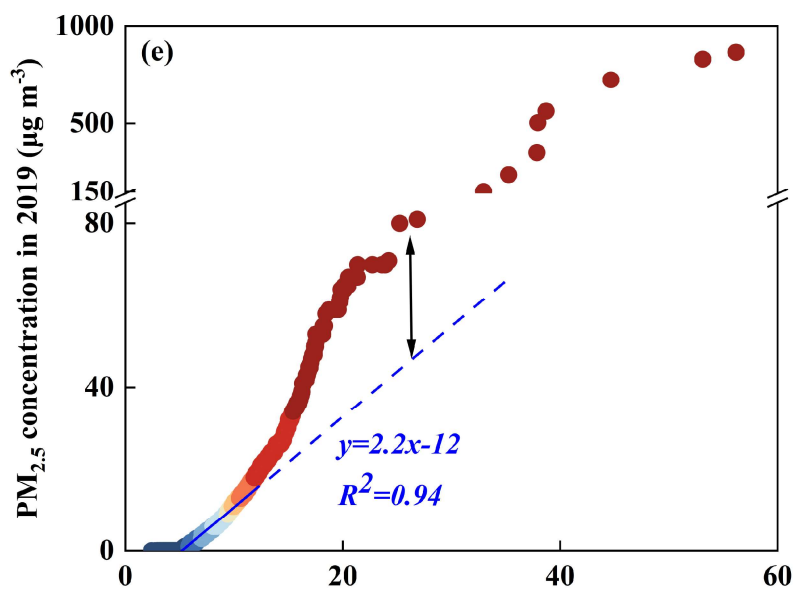
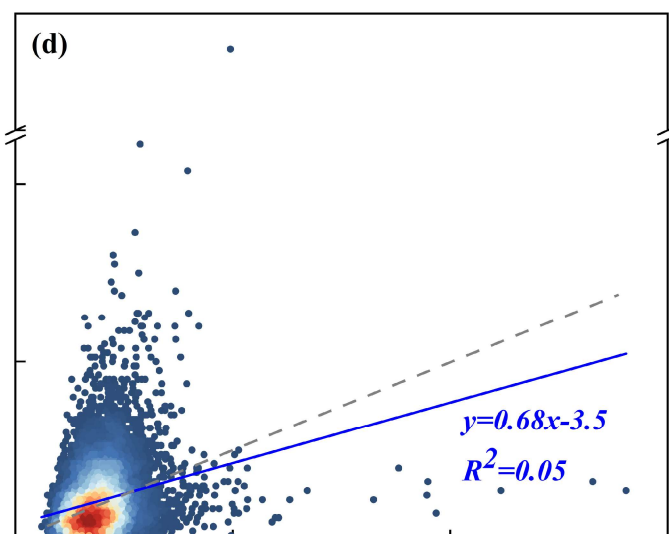
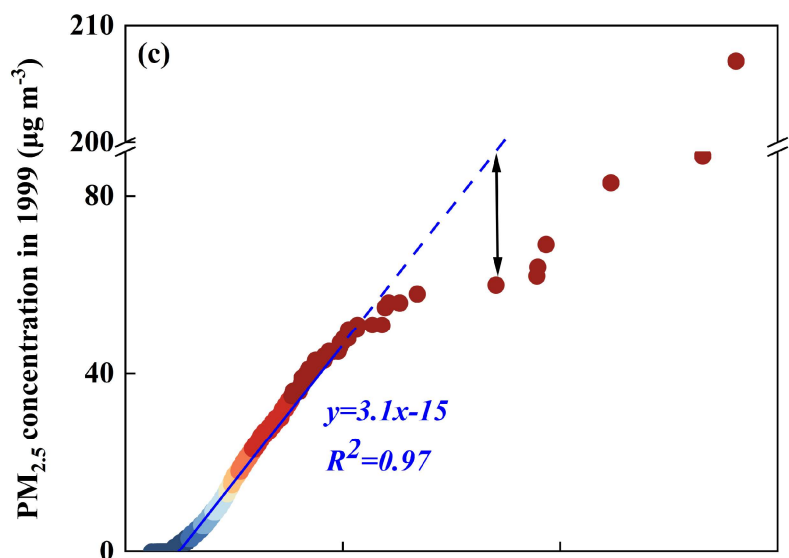
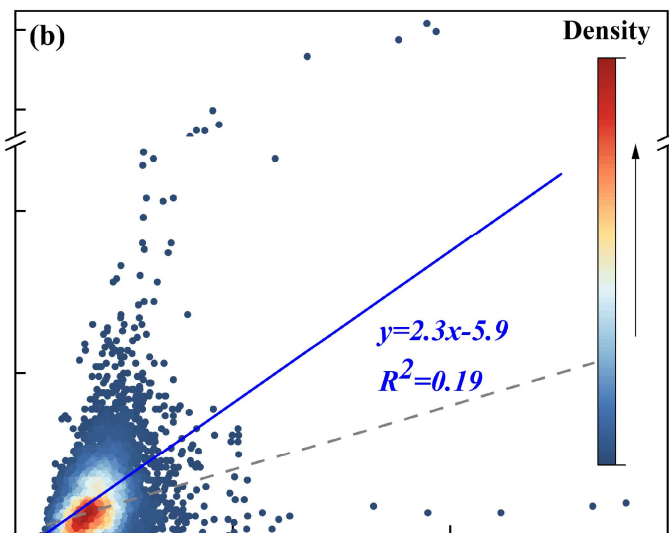
Fig. 5. The calculated perturbation contribution to the corresponding original annual average PM<sub>2.5</sub> concentration (left column) and the mean and standard derivation of the calculated perturbation (right column) in five western Canadian cities.



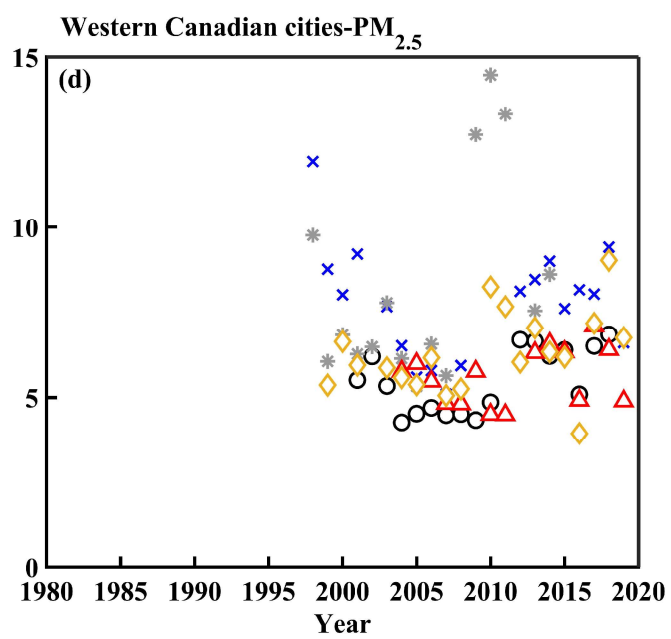
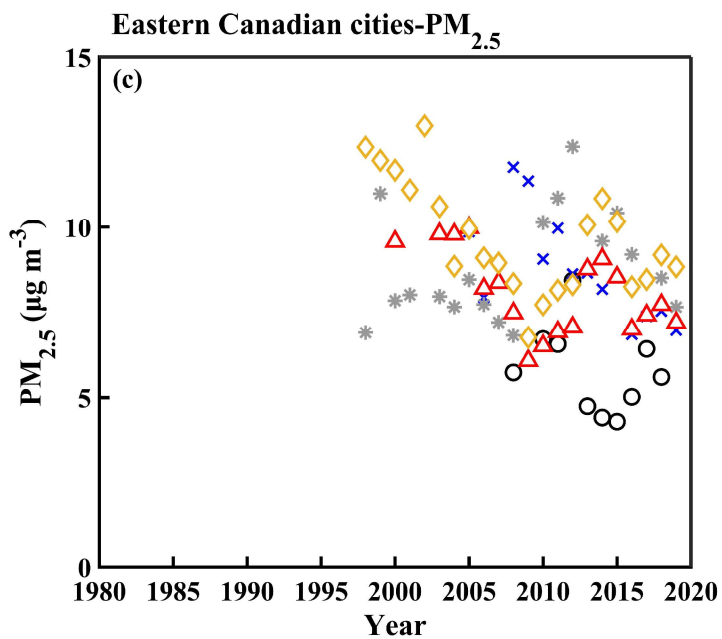
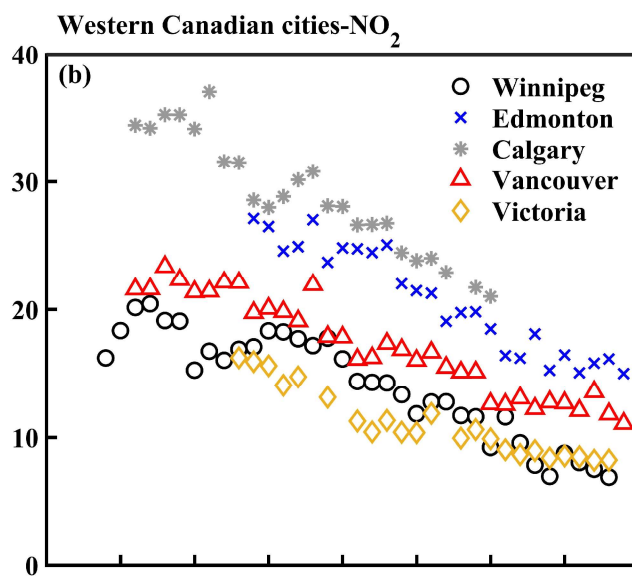
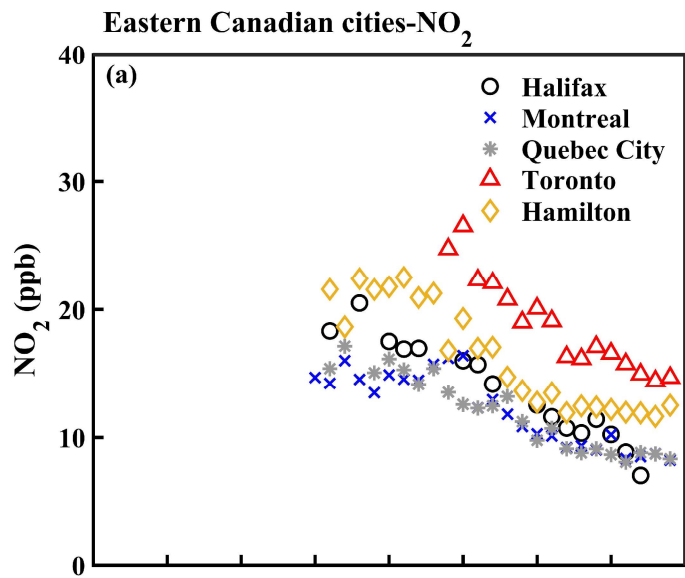
Percentile series

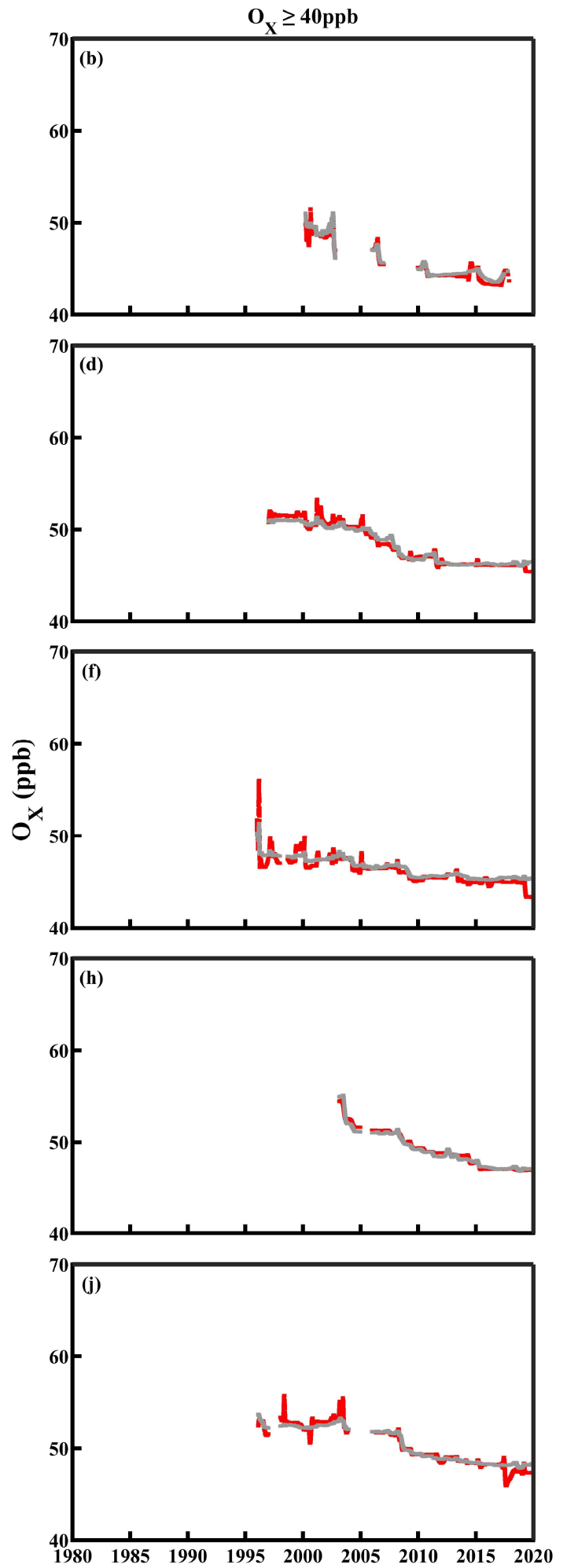
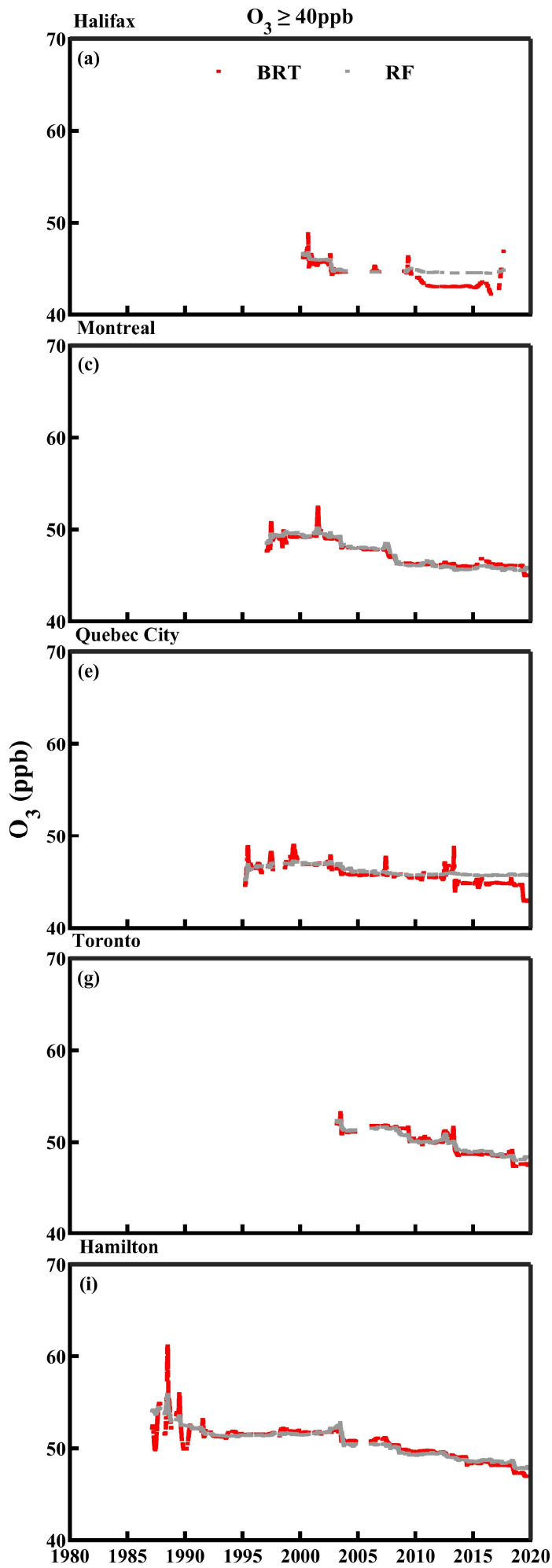


Time series



PM<sub>2.5</sub> concentration in 1998-2019 (22-year average in each hour) (μg m<sup>-3</sup>)





Year

